# Controllable and Constrained Sampling in Diffusion Models via Initial Noise Perturbation

Bowen  $Song^1$  Zecheng Zhang $^2$  Zhaoxu Luo  $^1$  Jason Hu  $^1$  Wei Yuan $^3$  Jing Jia $^4$  Zhengxu  $Tang^1$  Guanyang  $Wang^{3*}$  Livue  $Shen^{1*}$ 

#### **Abstract**

Diffusion models have emerged as powerful tools for generative tasks, producing high-quality outputs across diverse domains. However, how the generated data responds to the initial noise perturbation in diffusion models remains under-explored, which hinders understanding the controllability of the sampling process. In this work, we first observe an interesting phenomenon: the relationship between the change of generation outputs and the scale of initial noise perturbation is highly linear through the diffusion ODE sampling. Then we provide both theoretical and empirical study to justify this linearity property of this input-output (noisegeneration data) relationship. Inspired by these new insights, we propose a novel Controllable and Constrained Sampling (CCS) method, along with a new controller algorithm for diffusion models, that enables control over both the proximity of individual samples to a target image and the alignment of the sample mean with the target, while preserving good sample quality. We perform extensive experiments to compare our proposed sampling approach with other methods on both sampling controllability and sampled data quality. Results show that our CCS method achieves more precisely controlled sampling while maintaining superior sample quality and diversity, enhancing the applications of precise image editing. The code is available at https://github.com/efzero/diffusioncontroller.

#### 1 Introduction

Recently, diffusion models achieve remarkable success in generative tasks such as text-to-image generation, audio synthesis [24, 31], as well as conditional generation tasks including inverse problem solving, image or video restoration, image editing, and translation [3, 28, 44, 6, 34, 9, 26, 37, 20, 45]. Despite these success, real-world scientific and engineering problems pose more challenges on requesting reliable and controllable generation as well as data privacy.

To tackle this, one important question is: *How to control the distribution of samples from a diffusion model to match a specific target?* Previous works on controllable generation with diffusion models mostly focus on constraining the generation process sample-by-sample using either plug-and-play approaches [29, 9, 26, 37] or modifying the unconditional score [31, 45, 16, 6], so that each sample can satisfy a measurement constraint. However, most prior works focus on per-sample control, with limited exploration of how to regulate the overall distribution of generated samples to meet specific

 $Correspondence: Bowen Song \ (bowenbw@umich.edu), \ Guanyang \ Wang \ (guanyang.wang@rutgers.edu), \ and \ Liyue \ Shen \ (liyues@umich.edu)$ 

<sup>&</sup>lt;sup>1</sup>Department of Electrical Engineering and Computer Science, University of Michigan <sup>2</sup>TraceRoot.AI <sup>3</sup>Department of Statistics, Rutgers University <sup>4</sup>Department of Computer Science, Rutgers University

<sup>\*</sup>Joint senior authors.

statistical constraints, which is a crucial requirement in differential privacy [15]. This inspires the novel task for controllable and constrained sampling we are targeting in this paper. Considering the unique mechanism in diffusion sampling, we are motivated to exploit the initial noise control by studying this key question: *How do the initial noise perturbations affect the generated samples in diffusion models?* Previous works [2, 41] suggest that the learned posterior mean predictor function is locally linear with perturbation among a certain range of timesteps for diffusion models. However, this linearity cannot be applied to every timestep nor to the samples of diffusion models. From a new perspective, this work sheds lights on the relationship between input noise perturbations and generation data in diffusion models, by proposing a training-free approach.

First of all, we observe an interesting phenomenon that when using denoising diffusion implicit models (DDIM) sampling, the initial noise has a highly linear effect on the generation data at small or moderate scales. Motivated by this observation, our study tries to justify this linearity property via initial noise perturbation theoretically and empirically.

Based on the spherical interpolation to perturb the initial noise vector, we propose a novel *C*ontrollable and *C*onstrained *S*ampling method (*CCS*) for diffusion models to sample with a target rMSE level, enabling the sample mean to be close to the target image, while preserving high quality and adjustable diversity. The motivation for this task stems from a fundamental need in image editing and controllable generation: preserving key source features while allowing controlled variation. However, few studies benchmark sample quality and key feature preservation at a target controlled variation level. Our first key idea is to fix the average distance (rMSE) between samples and the target, enabling a fair comparison of sample diversity and feature preservation. Our second insight is to evaluate the distance between the sample mean and the target image, which reveals how well common features are preserved. In addition, our CCS algorithm enables a user-controllable "diversity slider": a tool that adjusts how far generated samples deviate from the input image. This fine-grained control over similarity can be vital for practical applications such as photo editing apps.

Furthermore, we conduct extensive experiments to validate the linearity phenomenon and then investigate the controllability performance of our proposed CCS method by generating images centered around a specified target mean image with a certain distance. Results demonstrate the superiority of our CCS method in both controllability and sampled image quality compared with baseline methods. Moreover, we show the potential of proposed CCS sampling for broader applications including precise image editing.

Our contributions can be summarized as below:

- We unveil a novel linear relationship between the initial noise and generated samples for DDIM sampling. We justify it theoretically, validate it thoroughly through extensive experiments, and discuss practical implications.
- We propose a novel task of controllable generation with the goal of making sample mean close to a target mean while controlling the MSE of samples to a target level. To the best of our knowledge, we are the first to study this task. This task can be useful for benchmarking the performance of personalized image generation.
- We propose a novel controllable sampling method based on our discovered linearity relationship.
   Extensive experiments with both pixel and latent diffusion models demonstrate the superior performance of our algorithm in achieving precise controllability within a our proposed constrained sampling framework.

# 2 Background

**Diffusion Models.** Diffusion models consists of a forward process that gradually adds noise to a clean image, and a reverse process that denoises the noisy images [35, 38]. The forward model is given by  $\mathbf{x}_t = \mathbf{x}_{t-1} - 0.5\beta_t\Delta t\mathbf{x}_{t-1} + \sqrt{\beta_t}\Delta t\omega$  where  $\omega \in \mathbb{N}(0,I)$  and  $\beta(t)$  is the noise schedule of the process. The distribution of  $\mathbf{x}_0$  is the clean data distribution, while the distribution of  $\mathbf{x}_T$  is approximately a standard Gaussian distribution. When we set  $\Delta t \to 0$ , the forward model becomes  $d\mathbf{x}_t = -0.5\beta_t\mathbf{x}_tdt + \sqrt{\beta_t}d\omega_t$ , which is a stochastic differential equation (SDE). The reverse of this SDE is given by:

$$dx_t = \left(-\frac{\beta(t)}{2} - \beta(t)\nabla_{\mathbf{x}_t} \log p_t(\mathbf{x}_t)\right) dt + \sqrt{\beta(t)} d\overline{\omega}.$$

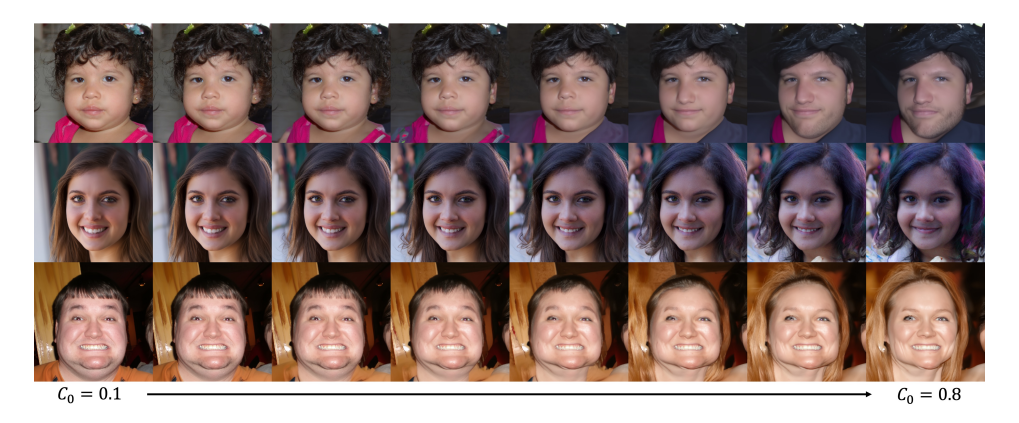


Figure 1: Qualitative demonstration of linearity when increasing scale of perturbation. For each target mean, we sample a perturbation noise and gradually increase  $C_0$  (0.1 at a time) to increase the magnitude of the perturbation.

One can training a neural network to learn the score function  $\nabla_{\mathbf{x}_t} \log p_t(\mathbf{x}_t)$ . However, this formulation involves running many timesteps with high randomness. We can also compute the equivalent Ordinary Differential Equation (ODE) form to the SDE, which has the same marginal distribution of  $p(\mathbf{x}_t)$ . A sampling process, called denoising diffusion implicit models (DDIM), modifies the forward process to be non-markovian, so as to form a deterministic probability-flow ODE for the reverse process [36]. In this way, we are able to achieve significant speed-up sampling. More discussion on this can be found in Section 3.

Constrained Generation with Diffusion Models. Constrained generation requires to sample  $\mathbf{x}_0$  subject to certain conditions or measurements  $\mathbf{y}$ . The conditional score at T can be computed by the Bayes rule, such that

$$\nabla_{\mathbf{x}_t} \log p_t(\mathbf{x}_t | \mathbf{y}) = \nabla_{\mathbf{x}_t} \log p_t(\mathbf{x}_t) + \nabla_{\mathbf{x}_t} \log p_t(\mathbf{y} | \mathbf{x}_t). \tag{1}$$

The second term can be computed through classifier guidance [13], where an external classifier is trained for  $p_0(\mathbf{y}|\mathbf{x}_0)$  or  $p_t(\mathbf{y}|\mathbf{x}_t)$ , and then can be plug into the diffusion model through Eq. 1. Diffusion posterior sampling [6] further refines this formulation by proposing to perform posterior sampling with the approximation of  $p(\mathbf{y}|\mathbf{x}_t) \approx p(\mathbf{y}|\hat{\mathbf{x}}_0)$ , where  $\hat{\mathbf{x}}_0$  is the Minimum Mean Square Error (MMSE) estimator of  $\mathbf{x}_0$  based on  $\mathbf{x}_t$ .

Another line of works exploit hard consistency, which projects the intermediate noise to a measurement-consistent space during sampling via optimization and plug-and-play [7, 9, 29, 34]. However, the projection term can damage the sample quality [6]. However, these works all target on controlling each individual sample. To our best knowledge, few works explore how to control the distribution of generated samples to match certain statistical constraints, such as centered around a specified target mean with certain distance, which is the target for this work.

Noise Perturbation in Diffusion Models. Noise adjustment for diffusion models has been explored in image editing, video generation, and other applications [28, 44, 10, 18, 42, 46] for changing the style or other properties of the generated data. However, a principled study on how the noise adjustment affects the samples is limited in diffusion models. Recently, [2, 41] observe the local linearity and low-rankness of the posterior mean predictor  $\hat{\mathbf{x}}_0$  based on  $\mathbf{x}_t$  in large timesteps, but this study cannot extend to the analysis of generated samples. In this work, we investigate how initial noise perturbations affect generated samples from the diffusion model in the ODE sampling setting.

# 3 Linear Relationship between Initial Noise and Outputs in Diffusion Models

This section analyzes how small perturbations in the input noise affect the generation data under the DDIM sampling framework. We show that a slight change in the initial noise leads to an approximately linear variation in the sampled images. This result is quantified from two perspectives: the discretized DDIM sampling process [36] and the associated continuous-time ODE. Our mathematical analysis

relies on minimal assumptions, which also serves as the foundation for our proposed CCS algorithm in Section 4.

# 3.1 Preliminary: DDIM Sampling

Fix the total sampling timesteps T and an initialization noise sample  $\mathbf{x}_T$ , [36] generates samples from the backward process  $\mathbf{x}_T \to \mathbf{x}_{T-1} \to \dots \to \mathbf{x}_0$  using the following recursive formula:

$$\mathbf{x}_{t-1} = \sqrt{\alpha_{t-1}} \left( \frac{\mathbf{x}_t - \sqrt{1 - \alpha_t} \, \epsilon_{\theta}^{(t)}(\mathbf{x}_t)}{\sqrt{\alpha_t}} \right) + \sqrt{1 - \alpha_{t-1} - \sigma_t^2} \, \epsilon_{\theta}^{(t)}(\mathbf{x}_t) + \sigma_t \epsilon_t, \tag{2}$$

where  $\alpha_t$  corresponds to the noise schedule in DDPM,  $\epsilon_{\theta}^{(t)}(\mathbf{x}_t)$  is the predicted noise given by the pretrained neural network with parameter  $\theta$ ,  $\epsilon_t$  is the standard Gaussian noise, and  $\sigma_t$  is a hyperparameter. The DDIM sampler [36] sets  $\sigma_t = 0$  to make the backward process deterministic once  $\mathbf{x}_T$  is fixed. It is known (e.g., eq (11) of [14]) that predicting the noise is equivalent to predicting the score function up to a normalizing factor, i.e.,  $\epsilon_{\theta}^{(t)}(\mathbf{x}_t) \approx -\sqrt{1-\alpha_t}\nabla_{\mathbf{x}_t}\log p_t(\mathbf{x}_t)$ . By setting  $\sigma_t = 0$  and substituting  $\epsilon_{\theta}^{(t)}$  with its corresponding estimand, we obtain the idealized DDIM process:

$$\mathbf{x}_{t-1} = \sqrt{\alpha_{t-1}} \left( \frac{\mathbf{x}_t + (1 - \alpha_t) \nabla_{\mathbf{x}_t} \log p_t(\mathbf{x}_t)}{\sqrt{\alpha_t}} \right) - \sqrt{(1 - \alpha_{t-1})(1 - \alpha_t)} \nabla_{\mathbf{x}_t} \log p_t(\mathbf{x}_t).$$
 (3)

If we treat the index t as a continuous variable (and rewrite  $\alpha_t$  as  $\alpha(t)$  to avoid confusion), we can write the idealized ODE as:

$$d\bar{\mathbf{x}}_t = -\sqrt{1 - \alpha(t)} \nabla \log p_t \left( \frac{\bar{\mathbf{x}}_t}{\sqrt{\sigma^2(t) + 1}} \right) d\sigma(t). \tag{4}$$

We now examine how a small perturbation  $\mathbf{x}_T \to \mathbf{x}_T + \lambda \Delta \mathbf{x}$  would affect the output sample at time t = 0 through both the discrete (3) and continuous time (4) perspectives.

**Related work:** Theorem 1 in [3] presents a related result on the impact of initial noise perturbation. Our study differs from theirs in a variety of aspects. Firstly, they study  $\mathbb{E}[\mathbf{x}_0 \mid \mathbf{x}_t + \lambda \Delta \mathbf{x}] - \mathbb{E}[\mathbf{x}_0 \mid \mathbf{x}_t]$  under the (stochastic) diffusion process. In contrast, we directly examine the output  $\mathbf{x}_0$  given the initializations  $\mathbf{x}_t$  and  $\mathbf{x}_t + \lambda \Delta \mathbf{x}$  under the deterministic DDIM (3) or the ODE process (4). Secondly, [3] assumes that  $p_0$  is a low-rank mixture of Gaussian distributions, which allows for an analytical solution for  $p_t$ . In contrast, our weaker assumptions render  $p_t$  analytically intractable. Consequently, we use very different techniques, such as ODE stability theory and Grönwall's inequality, to study the system's behavior.

# 3.2 Linearity in DDIM Discretizated Sampling

Previous works reveal the local linearity of the denoiser (which learns the score function) is quite strong [2, 27] in certain range of timesteps for diffusion models. Indeed, we can demonstrate that at very large noise levels, the score function is approximately linear. If a distribution is Gaussian, its score function is a linear function. Let:  $\mathbf{x} \sim \mathcal{N}(\mu, \Sigma)$  the score function is given by:  $\nabla_{\mathbf{x}} \log p(\mathbf{x}) = -\Sigma^{-1}(\mathbf{x} - \mu)$  which is linear in  $\mathbf{x}$ .

This explains why the denoiser exhibits high linearity at large timesteps as observed in [2, 27]. For DDPM, since  $\mathbf{x}_t = \sqrt{\alpha_t}\mathbf{x}_0 + \sqrt{1-\alpha_t}\,\epsilon$  where  $\epsilon \sim \mathcal{N}(0,I)$ , as t increases, the noise term dominates, and  $p(\mathbf{x}_t)$  approaches a Gaussian. Based on this observation, we can derive an approximately linear relationship between change and input initial noise and output of DDIM sampling as demonstrated in Proposition 1.

**Proposition 1.** With all the notations defined as above, assuming  $\log p_t$  is second-order differentiable for every  $t \geq 1$ , there exists a matrix-valued function  $\gamma_0$  such that

$$\mathbf{x}_0(\mathbf{x}_T + \lambda \Delta \mathbf{x}, T) = \mathbf{x}_0(\mathbf{x}_T, T) + \lambda \gamma_0(\mathbf{x}_T) \Delta \mathbf{x} + o(\lambda).$$

In turn,

$$\|\mathbf{x}_0(\mathbf{x}_T + \lambda \Delta \mathbf{x}, T) - \mathbf{x}_0(\mathbf{x}_T, T)\|_2 = \|\lambda \gamma_0(\mathbf{x}_T) \Delta \mathbf{x}\|_2 + o(\lambda).$$

Proposition 1 shows that a linear perturbation of the input with magnitude  $\lambda$  and direction  $\Delta \mathbf{x}$  results in an approximately linear change in the output, with magnitude  $|\lambda| || \gamma_0(\mathbf{x}_T) \Delta \mathbf{x} ||_2$  and direction  $\gamma_0(\mathbf{x}_T) \Delta \mathbf{x}$ . Recalling Eq. 2, each idealized DDIM sampling can be viewed as a linear combination of the current intermediate noisy input  $\mathbf{x}_t$  and the score function  $\nabla_{\mathbf{x}_t} \log p_t(\mathbf{x})$ . Based on this observation, Proposition 1 can be derived recursively using the linear approximation of the score function since each DDIM sampling step takes a linear combination of the predicted score and the intermediate noise. The derivation can be found in Appendix A.1. Our assumption is based solely on the second-order smoothness of the score, which is weaker than most existing assumptions depending on the data distribution  $p_0$ . For example, our assumptions hold under common conditions in the literature, such as the manifold hypothesis [11, 38] or the mixture of (low-rank) Gaussian assumption [17, 3, 1].

Furthermore, at large t,  $p_t$  is approximately Gaussian and  $\nabla_{\mathbf{x}_t} \log p_t(\mathbf{x}_t)$  is smooth, which implies small linear approximation error. The reason for the small error is that: 1) the score function of a Gaussian is linear in  $\mathbf{x}$  by  $\nabla_{\mathbf{x}} \log p(\mathbf{x}) = -\Sigma^{-1}(\mathbf{x} - \mu)$ , 2) when a function is smooth and its higher-order derivatives are small in magnitude, it has fewer abrupt changes, and the linear approximation error is bounded by the norm of the Hessian of the score function (through the Taylor Remainder Theorem), leading to low linear approximation error. However, one might be concerned that the linear approximation error could grow significantly when t decreases and  $p_0$  contains multiple clusters with low-density regions in between. Nevertheless, we now explain why this concern does not arise in practice. The coefficient  $f(t) := -\sqrt{\alpha_t}^{-1}\sqrt{\alpha_{t-1}(1-\alpha_t)} + \sqrt{1-\alpha_{t-1}}$  of  $\epsilon_{\theta}^{(t)}(\mathbf{x}_t)$  in (2) is close to 0 for small t, as  $\alpha_t \approx 1$ . Moreover, the structure of the neural network  $\epsilon_{\theta}$  ensures that the output is normalized and bounded in norm, so the change in output is also bounded. Consequently, for a small perturbation in  $\mathbf{x}_t$ , we have  $\|f(t)(\epsilon_{\theta}^{(t)}(\mathbf{x}_t + \Delta \mathbf{x}) - \epsilon_{\theta}^{(t)}(\mathbf{x}_t))\|_2 \approx 0$  when t is small. Linear Approximation Error. We provide further analysis of this linear approximation error in

**Linear Approximation Error.** We provide further analysis of this linear approximation error in the Appendix. We derive that this error is affected by the magnitude and the smoothness of local probability density  $p(x_0 = x_{\text{sample}})$ .

### 3.3 ODE Stability

Let  $\bar{\mathbf{x}}_0(\mathbf{x},T)$  be the solution of (4) with initialization  $\mathbf{x}_T = \mathbf{x}$  (i.e.,  $\bar{\mathbf{x}}_T = \mathbf{x}/\sqrt{\alpha(T)}$ ) at timestep T, and  $x_0(\mathbf{x},T) = \alpha(0)\bar{\mathbf{x}}_0(\mathbf{x},T)$ . With some technical assumptions that is detailed in Appendix, we have the following:

**Proposition 2.** There exists a matrix-valued function  $\psi_0$  such that:

$$\bar{\mathbf{x}}_0(\mathbf{x}_T + \lambda \Delta \mathbf{x}, T) = \bar{\mathbf{x}}_0(\mathbf{x}_T, T) + \lambda \psi_0(\mathbf{x}_T) \Delta \mathbf{x} + o(\lambda).$$

In turn,

$$\mathbf{x}_0(\mathbf{x}_T + \lambda \Delta \mathbf{x}, T) = \mathbf{x}_0(\mathbf{x}_T, T) + \lambda \sqrt{\alpha(0)} \psi_0(\mathbf{x}_T) \Delta \mathbf{x} + o(\lambda).$$

Proposition 2 mirrors Proposition 1 but is formulated in the continuous-time ODE setting. Its proof relies on ODE stability theory, showing that the output change is "approximately linear" for sufficiently small  $\lambda$ . Furthermore, under the same assumption, we establish that the change remains "at most linear" for all  $\lambda$ . The proof, which applies Grönwall's inequality, is provided in Appendix.

**Proposition 3.** With the same assumptions as above, there exists a constant C(T) depending on T such that for any  $\lambda$ :

$$\|\bar{\mathbf{x}}_0(\mathbf{x}_T + \lambda \Delta \mathbf{x}, T) - \bar{\mathbf{x}}_0(\mathbf{x}_T, T)\|_2 \le C(T) \|\lambda\| \|\Delta \mathbf{x}\|_2.$$

# 4 Sampling with Control

Our objective is to perturb  $\mathbf{x}_T$  into a random  $\mathbf{x}_T'$  such that the generated image  $\mathbf{x}_0'$  such that it has 1. a sample mean close to  $\mathbf{x}_0$  while maintaining 2. sufficient diversity and difference from the original image and 3. high image quality. We preserve the notation  $\mathbf{x}_0$  to denote a "target image" or "target mean". We also preserve the notation  $\mathbf{x}_T := \mathrm{DDIM}^{-1}(\mathbf{x}_0; 0, T)$ , the "noise" by finding a reliable initial noise  $\mathbf{x}_T$ , such that  $\mathrm{DDIM}(\mathbf{x}_T) = \mathbf{x}_0$  The closeness is quantified by L-2 norm distance  $\|\mathbb{E}[\mathbf{x}_0'] - \mathbf{x}_0\|_2$ , and the diversity is measured by  $\mathbb{E}[\|\mathbf{x}_0' - \mathbf{x}_0\|_2^2]$ . A notable feature of our algorithm is that users can specify a desired level of diversity (such as using  $C_0$  in Fig.1), and the generated images will match this level while ensuring  $\mathbb{E}[\mathbf{x}_0'] \approx \mathbf{x}_0$ . Our mechanism is defined as  $\mathbf{x}_T' = a\mathbf{x}_T + b\Delta$ , where  $\Delta$  is a random perturbation, and a and b are parameters to be specified shortly.

#### 4.1 Sampling around a Center

For an input of the form  $\mathbf{x}_T' = a\mathbf{x}_T + b\Delta$  with random  $\Delta$ , when b is small and a is close to 1, it can be regarded as a slight perturbation of  $\mathbf{x}_T$ . Based on Section 3, the output will remain close to  $\mathbf{x}_0$  with an additional linear adjustment applied to  $b\mathbf{n}$ . Thus, we define  $\hat{\mathbf{x}}_0' := \mathbf{x}_0 + bA\Delta$  as an approximation for  $\mathbf{x}_0'$ , where  $A = \gamma_0(a\mathbf{x}_T + b\Delta)$  specified in Proposition 1. Since  $\Delta$  is the only source of randomness in  $\hat{\mathbf{x}}_0'$ , we can easily calculate  $\mathbb{E}[\hat{\mathbf{x}}_0'] = \mathbf{x}_0 + bAE[\Delta]$  and  $\mathrm{Var}[\hat{\mathbf{x}}_0'] = b^2 A \mathrm{Cov}(\Delta)A^{\top}$ . We will now discuss the principles for our sampling design.

**High-quality image generation:** we first note that the input to both DDPM and DDIM samplers is standard Gaussian noise. The following feature is known as the "concentration phenomenon" of a high-dimensional Gaussian:

**Proposition 4.** Let  $X \sim \mathbb{N}(0, I_d)$ , then for any  $\delta \in (0, 1)$ 

$$\mathbb{P}\left[\|X\|_2^2 \in (1\pm\delta)d\big|\right] \geq 1 - 2\exp\left(-\frac{1}{2}d\left(\frac{1}{2}\delta^2 - \frac{1}{3}\delta^3\right)\right).$$

This result suggests that a standard Gaussian noise vector remains close to a hypersphere of radius  $\sqrt{d}$ .

Close to target mean: Our approximation  $\hat{\mathbf{x}}'_0$  has expectation  $\mathbb{E}[\hat{\mathbf{x}}'_0] = \mathbf{x}_0 + bAE[\Delta]$ . Thus, it is sufficient to select  $\Delta$  such that  $\mathbb{E}[\Delta] = 0$  in order to achieve:  $\mathbb{E}[\hat{\mathbf{x}}_0] \approx \mathbb{E}[\hat{\mathbf{x}}'_0] = \mathbf{x}_0$ , where the first approximation is justified by Proposition 1 and 2, with further empirical validation in Appendix.

# 4.2 Centering Feasibility

The simplest strategy is to add a random noise vector  $\Delta \mathbf{x}$  directly to  $\mathbf{x}_T$ , expressed as  $\mathbf{x}_T' = \mathbf{x}_T + \Delta \mathbf{x}$  (with  $a = 1, b\Delta = \Delta \mathbf{x}$ ). However, the following proposition demonstrates that this approach cannot produce high-quality images.

**Proposition 5.** For any fixed vector  $\mathbf{x}$ , and any random vector  $\Delta \mathbf{x}$  such that  $\mathbb{E}[\Delta \mathbf{x}] = 0$ , the following holds:

$$\mathbb{E}[\|\mathbf{x} + \Delta \mathbf{x}\|_2^2] = \|\mathbf{x}\|_2^2 + \operatorname{tr}(\operatorname{Cov}[\Delta \mathbf{x}]) \ge \|\mathbf{x}\|_2^2,$$

with equality if and only if  $\Delta \mathbf{x} = 0$  almost surely.

Proposition 5 indicates that directly adding noise,  $\mathbf{x}_T \to \mathbf{x}_T' := \mathbf{x}_T + \Delta \mathbf{x}$ , pushes  $\mathbf{x}_T'$  farther from the spherical surface. This partly explains why the average image becomes blurrier or noisier as the scale of  $\Delta \mathbf{x}$  increases, since the drift term  $\operatorname{tr}(\operatorname{Cov}[\Delta \mathbf{x}])$  grows larger, causing  $\mathbf{x}_T'$  to deviate further from the sphere with radius  $\|\mathbf{x}_T\|_2$ . On the other hand, a simple linear interpolation such as for also cannot produce high-quality images", because this will shrink the magnitude of the interpolated vector, which we demonstrate in the experiments. This inspires us to consider the spherical linear interpolation method [33] for sampling, as described below. Similar approaches have been proposed by [46, 35], but only for interpolating between two images.

# 4.3 Spherical Interpolation

Let vectors  $\mathbf{a}$  and  $\mathbf{b}$  satisfy  $\|\mathbf{a}\|_2 = \|\mathbf{b}\|_2$  and form an angle  $\theta$ . Then for any  $\alpha \in (0,1)$ , the vector obtained through spherical interpolation  $\mathbf{c} := \frac{\sin(\alpha\theta)}{\sin\theta}\mathbf{a} + \frac{\sin((1-\alpha)\theta)}{\sin(\theta)}\mathbf{b}$  satisfies  $\|\mathbf{c}\|_2 = \|\mathbf{a}\|_2 = \|\mathbf{b}\|_2$ . In our case, for a standard d-dimensional normal noise vector  $\epsilon$ , it is known  $\|\epsilon\|_2 \approx \sqrt{d} \approx \|\mathbf{x}_T\|_2$ . Therefore, we can do spherical interpolation between  $\mathbf{x}_T$  and  $\epsilon$  to obtain  $\mathbf{x}_T'$ . Our CCS algorithm is described in Algorithm 1.

The perturbation mechanism corresponds to  $\mathbf{x}_T' = a\mathbf{x}_T + b\Delta$  with  $a = \sin(\theta - C_0)/\sin(\theta)$ ,  $b = \sin(C_0)/\sin(\theta)$ , and  $\Delta$  is a

#### **Algorithm 2** Controller Tuning (CT)

1: Input: target mean  $\mathbf{x}_0$ , target diversity level MSE<sub>target</sub>, tolerance: tol,  $C_0$ , and  $C_{high}$ 2: Initialize:  $C_0 \leftarrow \frac{C_{\text{low}} + C_{\text{high}}}{2}$ 2: while not converged do

3: Sample a batch of  $\mathbf{x}'_0$  by Alg. 1

4: if  $|\mathbb{E}[||\mathbf{x}'_0 - \mathbf{x}_0||_2] - \text{MSE}_{\text{target}}| < \text{tol then}$ 5: Break

6: else if  $\mathbb{E}[||\mathbf{x}'_0 - \mathbf{x}_0||_2] > \text{MSE}_{\text{target}}$  then

7:  $(C_{\text{high}}, C_0) \leftarrow (C_0, \frac{C_0 + C_{\text{low}}}{2})$ 8: else

9:  $(C_{\text{low}}, C_0) \leftarrow (C_0, \frac{C_0 + C_{\text{high}}}{2})$ 10: end if

10: end while=0

### Algorithm 1 (Full Inversion) CCS Sampling

**Requires:** target mean  $x_0$ , perturbation scale  $C_0$ , number of diffusion model timesteps T

**Step 0:** Compute the DDIM inversion of  $\mathbf{x}_0$ , i.e.  $\mathbf{x}_T = \text{DDIM}^{-1}(\mathbf{x}_0, 0, T)$ 

**Step 1:** Sample noise  $\epsilon \sim \mathbb{N}(0, I)$ . Then compute

$$\theta = \cos^{-1} \left( \frac{\epsilon \cdot \mathbf{x}_T}{||\epsilon||_2 ||\mathbf{x}_T||_2} \right)$$

**Step 2:** Compute  $x_T$  using spherical interpolation formula:

$$\mathbf{x}_T' = \frac{\sin(C_0)}{\sin(\theta)} \cdot \epsilon + \frac{\sin(\theta - C_0)}{\sin(\theta)} \cdot \mathbf{x}_T$$

**Step 3:** Output sample  $\mathbf{x}'_0 = \text{DDIM}(\mathbf{x}'_T, T, 0)$ 

standard Gaussian noise.  $C_0 := \alpha \theta$  is defined as the parameter of perturbation scale. This mechanism satisfies the design principles described in Section 4.1:  $\mathbb{E}[\epsilon] = 0$  ensures that the new sample remains close to the target mean, while the Gaussian concentration and spherical interpolation ensure that  $\|\mathbf{x}_T'\|_2 \approx \|\mathbf{x}_T\|_2$ , resulting in high-quality generated images. Parameter  $C_0$  controls sampling diversity. In the extreme case  $C_0 = 0$ , we have  $\mathbf{x}_T' = \mathbf{x}_T$ , so  $\mathbf{x}_0'$  matches  $\mathbf{x}_0$  exactly but has no diversity. A larger  $C_0$  makes the perturbed input deviate more from the original image and gets closer to noise. This leads to greater diversity in the generated image.

Algorithm 2 allows users to control the desired level of diversity. It works by calling Alg. 1 for different values of  $C_0$ , which are determined through binary search. Let the process is repeated until the desired diversity level (up to a small tolerance threshold) is reached: if the MSE of generated images to target mean is below target threshold,  $C_0$  is increased; otherwise, it is decreased.

The following theorem demonstrates that the CCS algorithm is able to precisely control the input distance.

**Proposition 6.** Denote the dimensionality of  $\mathbf{x}_T$  by d. Given an initial noise  $\mathbf{x}_T$  with  $\|\mathbf{x}_T\|_2 = (1+o(1))\sqrt{d}$ , and fix a small  $\delta > 0$ . For any  $M \leq (2-\delta)\sqrt{d}$ , then we can find  $C_0$  in Algorithm 1 such that with probability  $p_d \to 1$  as  $d \to \infty$ , we have  $\|\mathbf{x}_T' - \mathbf{x}_T\|_2 = M$ .

Since the dimensionality of our problem is sufficiently large, Proposition 6 allows users to control M as the input distance. Consequently, Algorithm 1 can generate a random interpolants with an exact distance of M from the input. Furthermore, since the direction is uniformly distributed, and when  $C_0$  is small,  $\mathbb{E}[\mathbf{x}_T'] \approx \mathbb{E}[\mathbf{x}_T]$ , and  $\mathbb{E}[\mathbf{x}_0'] \approx \mathbb{E}[\mathbf{x}_0]$ , which satisfies our design goal.

In other cases when the inverted noise does not lie on the standard Gaussian hypersphere, we argue that our proposed spherical interpolation leads the second moment closer to a standard Gaussian. Formally, Fix any vector  $\mathbf{x} \in \mathbb{R}^d$ , and let  $\epsilon \sim \mathbb{N}(0, I_d)$ . Let  $\theta \in [0, \pi]$  be the angle between  $\mathbf{x}$  and  $\epsilon$ . We define the interpolated vector:

$$\mathbf{y} = \frac{\sin(c\theta)}{\sin(\theta)} \epsilon + \frac{\sin((1-c)\theta)}{\sin\theta} \mathbf{x}.$$

Our goal is to show y is closer than x to a Gaussian in the second-moment (energy-shell) sense. Since a standadrd Gaussian has second moment  $\mathbb{E}[||Z||^2] = d$ , we define the gap of second moment as:

$$\delta(Y) := |\mathbb{E}[Y^2] - d|.$$

**Proposition 7.** For any  $c \in (0,1)$ , we have:

$$\delta(\mathbf{y}) \leq \delta(\mathbf{x}).$$

In summary, we argued that we can center our samples around the target mean better through spherical interpolation with random noise as in Prop. 5, and control the distance to the sample mean through adjusting the perturbation scale  $C_0$  as in Prop. 6, and we can also improves the sample quality even if the initial noise is not on a Gaussian hypersphere as demonstrated in Prop. 7.

#### 4.4 Extension to Conditional Latent Diffusion Models

Conditional diffusion models usually compute the conditional score with classifier-free guidance (CFG). Let  $s_{\theta}(\mathbf{x}_t,t)$  be the predicted noise, it can be written in  $s_{\theta}(\mathbf{x}_t,t) = s_{\theta}(\mathbf{x}_t,t,c_{null}) + \gamma(s_{\theta}(\mathbf{x}_t,t,c) - s_{\theta}(\mathbf{x}_t,t,c_{null}))$  where  $\gamma$  is the CFG term, c is the condition and  $c_{null}$  is the null condition. The computation is more expensive, and we may not want to change the semantics drasticly by a small perturbation. Motivated by this, we propose a Partial-Inversion CCS Sampling algorithm (P-CCS). Instead of starting from the T, we pick an intermediate timestep  $t_0$ . Then, we compute the noise term from DDIM inversion by subtracting the clean component, sample a new noise from  $\mathbb{N}(0,(1-\alpha_{t_0})I)$ , and then perform spherical interpolation. Details of this partial inversion algorithm (P-CCS) can be found in the Appendix.

# 5 Applications and Experiments

In this section, we will discuss the applications of the observed linearity property with the proposed controllable sampling techniques.

# **5.1** Linearity Property

**Experimental Validation.** We perform extensive experiments on both pixel diffusion models on the FFHQ and CIFAR-10 dataset and latent diffusion models on the Celeba-HQ and fMoW dataset. For

Table 1:  $\mathbb{R}^2$  between input perturbation and normalized residual norms

Pixel Dif	fusion Models	<b>Latent Diffus</b>	ion Models
FFHQ	CIFAR-10	CelebA-HQ	fMoW
0.995	0.988	0.959	0.947

each experiment, we first sample 50 images as target images from each validation dataset from FFHQ [22], CIFAR-10 [25], and Celeba-HQ [43]. We also pick one images each class from the validation set of the fMoW dataset [5] for further verification. Then for the FFHQ and CIFAR-10 selected data, we use pixel diffusion models as backbone; for Celeba-HQ and fMoW we use stable diffusion 1.5 as the backbone. For each target image, we sample eight  $C_0$  from a uniform [0, 0.9] distribution. For each  $C_0$ , we sample 24 images. Then we compute the average  $L^2$  distance between the sampled images and the target mean for each scale. We compute the R-squared coefficient ( $R^2$ ) between the input perturbation scales and the normalized average residual norms (scale between 0-1). As shown in Table 4, we observe a very strong linearity in the above experiments. Fig. 1 also demonstrates linear semantic change visually. We provide additional analysis in the Appendix. In summary, the linearity widely exists for DDIM sampling regardless of dataset or model backbone, and it may heavily depend on the dataset distribution.

To further investigate how the linearity changes with the complexity of dataset, and different diffusion model backbones. We perform experiments to test the linearity of (1) pretrained diffusion models on a simple dataset such as FFHQ. (2) pretrained diffusion models on multimodal dataset (with many classes) such as ImageNet. (3) large pretrained foundation models such as Stable Diffusion Model (trained on complex multimodal dataset). We hypothesize that the linearity on out-of-distribution dataset will decreases, so we test the pretrained pixel-diffusion models on OOD datasets. While the training data for SD1.5 is very large (LAION-5B), we just test it on other multimodal datasets such as UCF-101 [39]

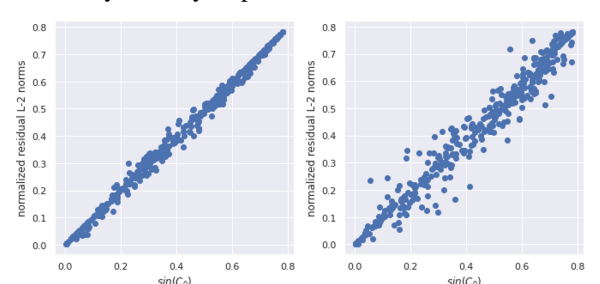


Figure 2: Quantitative demonstration of linearity when increasing scale of perturbation. With increased  $\sin(C_0)$ , the magnitude of perturbation increases, and the average  $L^2$  distance between samples and the target image increases linearly. Left is the linearity on FFHQ dataset using pixel diffusion; Right is the linearity on Celeba-HQ dataset using Stable Diffusion 1.5.

and ImageNet [12]. Results show that the linearity decreases significantly when testing on OOD dataset for pixel-diffusion models. For foundation models, complexity of dataset for sampling does not affect the linearity significantly. The linearity decreases slightly comparing diffusion models trained on multimodal dataset to those trained on simple dataset. These results validate the analysis in the linear approximation error, and imply that a low probability density and a sudden change in the

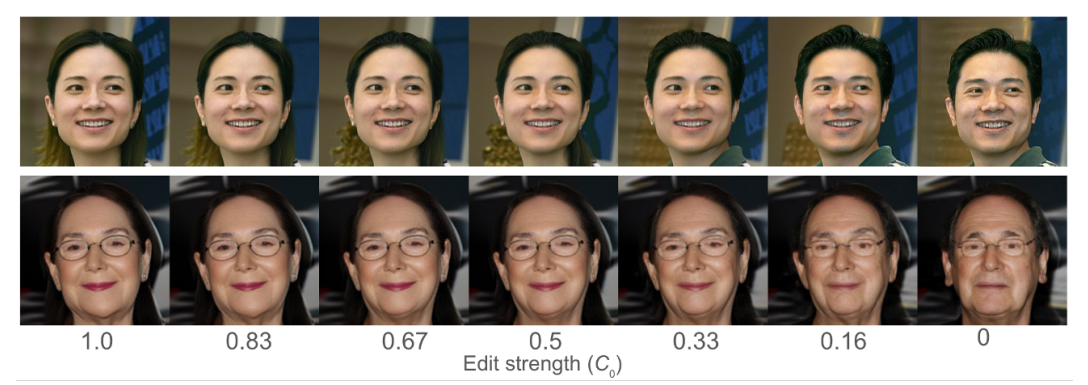


Figure 3: Precise image editing with the proposed P-CCS algorithm. Source prompt: "A high-quality portrait of a man". Target prompt: "A high-quality portrait of a woman". The right-most images with edit strength as 0 are the source images.

data distribution may contribute to low linearity. We also find significant drop of sample quality with low linearity. Details and numbers can be found in the Appendix.

**Application 1: Precise Image Editing.** With the aid of linearity property, we can perform the application of precise image editing, by having the user enters a value of edit strength to precisely control the target image edited to that extent. The key idea is through the DDIM inversion to project both the source and target images back to the initial noise manifold. Specifically, we first compute  $x_T^{(1)} = \text{DDIM}^{-1}(x_0, c_{\text{source}}), x_T^{(2)} = \text{DDIM}^{-1}(x_0, c_{\text{target}}),$  and then perform spherical interpolation between  $x_T^{(1)}$ , and  $x_T^{(2)}$  according to the user-specified editing strength. This is implemented using the proposed P-CCS algorithm with more details described in the Appendix (Alg. 4). As shown of two example images in Fig. 3, our algorithm can easily achieve a smooth and precise image editing guaranteed by the aforementioned linearity property.

# 5.2 Controllable Sampling

We propose CCS (Alg. 1) and P-CCS (Alg. 3) algorithms for controllable sampling close to a specified target image, constrained by a target MSE to the target mean. We validate that our algorithm can achieve this better than baselines while preserving good image quality. In addition, we demonstrate our algorithm's capability in generating personalized albums and improving sample quality.

**Application 2: Generating Personalized Album.** We perform experiments on generating personalized albums using both pixel diffusion models and latent diffusion models with our (P-)CCS algorithms. For benchmarking performance of different baselines, we propose a novel task of fixing MSE to a target image, and compare other metrics, which we call *controllable sampling*. The goal is to sample images as close to source as possible while keeping target diversity (MSE).

**Experimental setup:** We FFHQ-256 [22] and CelebA-HQ [43] test set images as target images. We use ADM (a pixel diffusion model) for FFHQ, and Stable Diffusion for CelebA-HQ. **Baselines:** We self-implement 5 baselines as comparison since no existing work is designed for the target task so some adaptation is necessary. Naive Linear interpolation with Controller (*LP-C*), Gaussian



Figure 4: We sample 120 images with a fixed target mean using different methods and analyze their sample mean (average pixel intensity). Our observations show that the sample mean of our method closely matches that of the original image.

Perturbation with Controller (*GP-C*), Diffusion Posterior Sampling [6] with Controller (*DPS-C*), ILVR with Controller (*ILVR-C*), Come-Closer-Diffuse-Faster with Controller (*CCDF-C* or *SDEdit-C*). **Metrics:** We adopt Peak Signal to Noise ratio (PSNR) for measuring whether sample mean is close to target

Table 2: Results of Pixel Diffusion models on the FFHQ Dataset with target rMSE set as 0.12.

Method	PSNR↑	SD↑	CLIP-IQA↑	MUSIQ↑
GP-C	18.88	0.028	0.701	45.88
ILVR-C	20.04	0.070	0.746	62.45
DPS-C	21.02	0.069	0.738	64.60
CCDF-C	<u>23.52</u>	0.088	<u>0.746</u>	<u>66.15</u>
CCS (Ours)-C	25.13	0.104	0.750	66.79

mean; LPIPS for measuring samples similarity to the source image; CLIP-IQA and MUSIQ for semantic/low-level image quality respectively; Standard Deviation (SD) for measuring sampling diversity. More experimental details and baseline implementation can be found in the Appendix.

Results. We observe that our CCS sampling method significantly outperforms all other methods in centering at a target mean constrained by a fixed rMSE distance, while surprisingly maintaining superior image perceptual quality and diversity. Other posterior sampling meth-

Table 3: Results of the Stable Diffusion 1.5 on the CelebA-HQ dataset with target rMSE set as 0.07.

Method	PSNR↑	SD↑	CLIP-IQA↑	MUSIQ↑
GP-C	23.02	0.045	0.721	48.91
LDPS-C	24.56	0.034	0.721	29.07
CCDF-C	<u>27.66</u>	<u>0.051</u>	0.735	<u>49.29</u>
CCS (Ours)-C	30.29	0.053	0.732	49.66

ods such as DPS suffer from image quality degradation and diversity decrease, as shown by the quantitative results reported in Table. 2 and 3. . Qualitatively, we observe that the sample means of other methods look blurry or noisy, as demonstrated in Fig. 4. More qualitative results can be found in the Appendix.

Application 3: Improving Image Quality through P-CCS Sampling. Note that in our (P-)CCS sampling algorithms, we perform spherical interpolation with a random Gaussian noise. Intuitively, if the initial noise is not Gaussian like falling in low-density probability region, conducting such interpolation will make it "more Gaussian" to increase the likelihood of that sample so as to enhance image qual-



make it "more Gaussian" to increase the likelihood of that sample so as to enhance image qual
Figure 5: Top: Corrupted images with artifacts or unreasonable structures. Bottom: Improved images by P-CCS algorithm through spherical interpolation of initial noises.

ity. We provide a formal argument for this in the Appendix. Motivated by this, we propose to perform P-CCS at some timesteps of reverse DDIM sampling. As shown in Fig. 5, we observe that the sample quality can be improved significantly by this simple method, which supports the potential of our findings to introduce a new post-training mechanism for enhancing image generation. More experiment details and quantitative results are described in the Appendix.

# 6 Conclusion

In this work, we unveil an interesting linear response to perturbation phenomenon both theoretically and empirically in diffusion models. we also study a new problem: how to sample images with a target mean and target MSE. We present a novel sampling algorithm along with a new controller method for achieving this goal. Extensive experiments show that our proposed method samples the closest to the target mean when controlling the MSE compared to other methods, while maintaining superior image quality and diversity. The limitations of our work include: (1) Controlling other interesting statistical properties beyond sample mean with MSE is left as future works. (2) There might be some artifact samples that exhibit overlapping patterns. (3) DDIM inversion may not be perfectly standard Gaussian, which may hurt sample quality. We believe the linearity property will be important for designing better latent space for large-scale diffusion models.

# Acknowledgments

LS acknowledges funding supports from National Science Foundation (NSF) (IIS-2435746), Defense Advanced Research Projects Agency (DARPA), Hyundai America Technical Center, Inc. (HATCI), University of Michigan MICDE Catalyst Grant Award and MIDAS PODS Grant Award. GW acknowledges support from the National Science Foundation (NSF) (DMS-2210849) and the Adobe Data Science Award.

#### References

- [1] Sitan Chen, Vasilis Kontonis, and Kulin Shah. Learning general gaussian mixtures with efficient score matching. *arXiv* preprint arXiv:2404.18893, 2024.
- [2] Siyi Chen, Huijie Zhang, Minzhe Guo, Yifu Lu, Peng Wang, and Qing Qu. Exploring low-dimensional subspace in diffusion models for controllable image editing. In *The Thirty-eighth Annual Conference on Neural Information Processing Systems*.
- [3] Siyi Chen, Huijie Zhang, Minzhe Guo, Yifu Lu, Peng Wang, and Qing Qu. Exploring low-dimensional subspace in diffusion models for controllable image editing. In *The Thirty-eighth Annual Conference on Neural Information Processing Systems*, 2024.
- [4] Jooyoung Choi, Sungwon Kim, Yonghyun Jeong, Youngjune Gwon, and Sungroh Yoon. Ilvr: Conditioning method for denoising diffusion probabilistic models. In *Proceedings of the IEEE/CVF International Conference on Computer Vision*, pages 14367–14376, 2021.
- [5] Gordon Christie, Neil Fendley, James Wilson, and Ryan Mukherjee. Functional map of the world. In *CVPR*, 2018.
- [6] Hyungjin Chung, Jeongsol Kim, Michael Thompson Mccann, Marc Louis Klasky, and Jong Chul Ye. Diffusion posterior sampling for general noisy inverse problems. In *The Eleventh International Conference on Learning Representations*.
- [7] Hyungjin Chung, Byeongsu Sim, Dohoon Ryu, and Jong Chul Ye. Improving diffusion models for inverse problems using manifold constraints. *Advances in Neural Information Processing Systems*, 35:25683–25696, 2022.
- [8] Hyungjin Chung, Byeongsu Sim, and Jong Chul Ye. Come-closer-diffuse-faster: Accelerating conditional diffusion models for inverse problems through stochastic contraction. In *Proceedings* of the IEEE/CVF Conference on Computer Vision and Pattern Recognition, pages 12413–12422, 2022.
- [9] Hyungjin Chung, Jong Chul Ye, Peyman Milanfar, and Mauricio Delbracio. Prompt-tuning latent diffusion models for inverse problems. *arXiv preprint arXiv:2310.01110*, 2023.
- [10] Jiwoo Chung, Sangeek Hyun, and Jae-Pil Heo. Style injection in diffusion: A training-free approach for adapting large-scale diffusion models for style transfer. In *Proceedings of the IEEE/CVF Conference on Computer Vision and Pattern Recognition*, pages 8795–8805, 2024.
- [11] Valentin De Bortoli. Convergence of denoising diffusion models under the manifold hypothesis. *Transactions on Machine Learning Research*, 2022.
- [12] Jia Deng, Wei Dong, Richard Socher, Li-Jia Li, Kai Li, and Li Fei-Fei. Imagenet: A large-scale hierarchical image database. In *Proceedings of the 2009 IEEE Conference on Computer Vision and Pattern Recognition (CVPR)*, pages 248–255. IEEE, 2009.
- [13] Prafulla Dhariwal and Alexander Nichol. Diffusion models beat gans on image synthesis. *Advances in neural information processing systems*, 34:8780–8794, 2021.
- [14] Prafulla Dhariwal and Alexander Nichol. Diffusion models beat GANs on image synthesis. *Advances in neural information processing systems*, 34:8780–8794, 2021.
- [15] Cynthia Dwork. Differential privacy. In *International colloquium on automata, languages, and programming*, pages 1–12. Springer, 2006.

- [16] Dave Epstein, Allan Jabri, Ben Poole, Alexei Efros, and Aleksander Holynski. Diffusion self-guidance for controllable image generation. *Advances in Neural Information Processing Systems*, 36:16222–16239, 2023.
- [17] Khashayar Gatmiry, Jonathan Kelner, and Holden Lee. Learning mixtures of gaussians using diffusion models. arXiv preprint arXiv:2404.18869, 2024.
- [18] Xiefan Guo, Jinlin Liu, Miaomiao Cui, Jiankai Li, Hongyu Yang, and Di Huang. Initno: Boosting text-to-image diffusion models via initial noise optimization. In *Proceedings of the IEEE/CVF Conference on Computer Vision and Pattern Recognition*, pages 9380–9389, 2024.
- [19] Philip Hartman. Ordinary differential equations. SIAM, 2002.
- [20] Yutong He, Naoki Murata, Chieh-Hsin Lai, Yuhta Takida, Toshimitsu Uesaka, Dongjun Kim, Wei-Hsiang Liao, Yuki Mitsufuji, J Zico Kolter, Ruslan Salakhutdinov, et al. Manifold preserving guided diffusion. In *The Twelfth International Conference on Learning Representations*.
- [21] Kaiyi Huang, Kaiyue Sun, Enze Xie, Zhenguo Li, and Xihui Liu. T2i-compbench: A comprehensive benchmark for open-world compositional text-to-image generation. Advances in Neural Information Processing Systems, 36:78723–78747, 2023.
- [22] Tero Karras. A style-based generator architecture for generative adversarial networks. *arXiv* preprint arXiv:1812.04948, 2019.
- [23] Junjie Ke, Qifei Wang, Yilin Wang, Peyman Milanfar, and Feng Yang. Musiq: Multi-scale image quality transformer. In *Proceedings of the IEEE/CVF international conference on computer* vision, pages 5148–5157, 2021.
- [24] Zhifeng Kong, Wei Ping, Jiaji Huang, Kexin Zhao, and Bryan Catanzaro. Diffwave: A versatile diffusion model for audio synthesis. In *International Conference on Learning Representations*.
- [25] Alex Krizhevsky, Geoffrey Hinton, et al. Learning multiple layers of features from tiny images. 2009.
- [26] Taesung Kwon and Jong Chul Ye. Solving video inverse problems using image diffusion models. *arXiv preprint arXiv:2409.02574*, 2024.
- [27] Xiang Li, Yixiang Dai, and Qing Qu. Understanding generalizability of diffusion models requires rethinking the hidden gaussian structure. *Advances in neural information processing systems*, 37:57499–57538, 2024.
- [28] Haofeng Liu, Chenshu Xu, Yifei Yang, Lihua Zeng, and Shengfeng He. Drag your noise: Interactive point-based editing via diffusion semantic propagation. In *Proceedings of the IEEE/CVF Conference on Computer Vision and Pattern Recognition*, pages 6743–6752, 2024.
- [29] Sai Shankar Narasimhan, Shubhankar Agarwal, Litu Rout, Sanjay Shakkottai, and Sandeep P Chinchali. Constrained posterior sampling: Time series generation with hard constraints. arXiv preprint arXiv:2410.12652, 2024.
- [30] Alexander Quinn Nichol and Prafulla Dhariwal. Improved denoising diffusion probabilistic models. In *International conference on machine learning*, pages 8162–8171. PMLR, 2021.
- [31] Robin Rombach, Andreas Blattmann, Dominik Lorenz, Patrick Esser, and Björn Ommer. High-resolution image synthesis with latent diffusion models. In *Proceedings of the IEEE/CVF conference on computer vision and pattern recognition*, pages 10684–10695, 2022.
- [32] Tim Salimans, Ian Goodfellow, Wojciech Zaremba, Vicki Cheung, Alec Radford, and Xi Chen. Improved techniques for training gans. Advances in neural information processing systems, 29, 2016.
- [33] Ken Shoemake. Animating rotation with quaternion curves. In *Proceedings of the 12th annual conference on Computer graphics and interactive techniques*, pages 245–254, 1985.

- [34] Bowen Song, Soo Min Kwon, Zecheng Zhang, Xinyu Hu, Qing Qu, and Liyue Shen. Solving inverse problems with latent diffusion models via hard data consistency. In *The Twelfth International Conference on Learning Representations*.
- [35] Jiaming Song, Chenlin Meng, and Stefano Ermon. Denoising diffusion implicit models. *arXiv* preprint arXiv:2010.02502, 2020.
- [36] Jiaming Song, Chenlin Meng, and Stefano Ermon. Denoising diffusion implicit models. In *International Conference on Learning Representations*, 2021.
- [37] Jiaming Song, Qinsheng Zhang, Hongxu Yin, Morteza Mardani, Ming-Yu Liu, Jan Kautz, Yongxin Chen, and Arash Vahdat. Loss-guided diffusion models for plug-and-play controllable generation. In *International Conference on Machine Learning*, pages 32483–32498. PMLR, 2023.
- [38] Yang Song and Stefano Ermon. Generative modeling by estimating gradients of the data distribution. *Advances in neural information processing systems*, 32, 2019.
- [39] Khurram Soomro, Amir Roshan Zamir, and Mubarak Shah. Ucf101: A dataset of 101 human actions classes from videos in the wild. *CoRR*, abs/1212.0402, 2012.
- [40] Jianyi Wang, Kelvin CK Chan, and Chen Change Loy. Exploring clip for assessing the look and feel of images. In *Proceedings of the AAAI Conference on Artificial Intelligence*, volume 37, pages 2555–2563, 2023.
- [41] Peng Wang, Huijie Zhang, Zekai Zhang, Siyi Chen, Yi Ma, and Qing Qu. Diffusion models learn low-dimensional distributions via subspace clustering. *arXiv preprint arXiv:2409.02426*, 2024.
- [42] Chen Henry Wu and Fernando De la Torre. A latent space of stochastic diffusion models for zero-shot image editing and guidance. In *Proceedings of the IEEE/CVF International Conference on Computer Vision*, pages 7378–7387, 2023.
- [43] Weihao Xia, Yujiu Yang, Jing-Hao Xue, and Baoyuan Wu. Tedigan: Text-guided diverse face image generation and manipulation. In *IEEE Conference on Computer Vision and Pattern Recognition (CVPR)*, 2021.
- [44] Jiaxin Zhang, Kamalika Das, and Sricharan Kumar. On the robustness of diffusion inversion in image manipulation. In ICLR 2023 Workshop on Trustworthy and Reliable Large-Scale Machine Learning Models, 2023.
- [45] Lvmin Zhang, Anyi Rao, and Maneesh Agrawala. Adding conditional control to text-to-image diffusion models. In *Proceedings of the IEEE/CVF International Conference on Computer Vision*, pages 3836–3847, 2023.
- [46] PengFei Zheng, Yonggang Zhang, Zhen Fang, Tongliang Liu, Defu Lian, and Bo Han. Noised-iffusion: Correcting noise for image interpolation with diffusion models beyond spherical linear interpolation. In *The Twelfth International Conference on Learning Representations*, 2024.

#### A Proofs

#### A.1 Proof in Section 3.2

Proof of Proposition 1. Let  $L_t(\mathbf{x}) := \eta_t \mathbf{x} + \lambda_t \nabla_{\mathbf{x}_t} \log p_t(\mathbf{x})$  be the one-step recursion. Our  $\mathbf{x}_0(a,t)$  is formally defined as  $L_1 \circ L_2 \circ \ldots \circ L_T(a)$ .

The second-order differentiability of  $p_t$  implies the score function  $\nabla \log p_t$  is first-order differentiable. Let  $H_t$  be the Hessian matrix of  $\log p_t$   $(H_t^{i,j} := \partial^2 \log p_t / \partial_i \partial_j)$ . We have

$$\nabla \log p_t(\mathbf{x}) = \nabla \log p_t(\mathbf{w}) + H_t(\mathbf{w})(\mathbf{x} - \mathbf{w}) + o(\|\mathbf{x} - \mathbf{w}\|_2).$$

Therefore, for any fixed direction w of unit length and  $\delta \in \mathbb{R}$ ,

$$L_{T}(\mathbf{x} + \delta \mathbf{w}) = \eta_{T}(\mathbf{x} + \delta \mathbf{w}) + \lambda_{T} \nabla_{\mathbf{x}} \log p_{T}(\mathbf{x} + \delta \mathbf{w})$$

$$= \eta_{T} \mathbf{x} + \lambda_{T} \nabla_{\mathbf{x}} \log p_{T}(\mathbf{x}) + \lambda_{T} \delta H_{T}(\mathbf{x}) \mathbf{w} + \delta \eta_{T} \mathbf{w} + o(\delta)$$

$$= L_{T}(\mathbf{x}) + \delta (\eta_{T} + \lambda_{T} H_{T}(\mathbf{x})) \mathbf{w} + o(\delta)$$

$$= L_{T}(\mathbf{x}) + \delta \gamma_{T}(\mathbf{x}) \mathbf{w} + o(\delta)$$

where  $\gamma_T(\mathbf{x})$  is defined as

$$\gamma_T(\mathbf{x}) = \eta_T + \lambda_T H_T(\mathbf{x}),$$

is a matrix-valued function which is bounded if the norm of the Hessian of  $\log p_t$  is bounded.

Applying  $L_{T-1}$  on both sides of the above formula:

$$\begin{split} L_{T-1} \circ L_T(\mathbf{x} + \delta \mathbf{w}) &= L_{T-1} \circ (L_T(\mathbf{x}) + \delta \gamma_T(\mathbf{x}) \mathbf{w} + o(\delta)) \\ &= \eta_{T-1} L_T(\mathbf{x}) + \delta \eta_{T-1} \gamma_T(\mathbf{x}) \mathbf{w} + o(\delta) + \lambda_{T-1} \nabla \log p_{T-1} \bigg( L_T(\mathbf{x}) + \delta \gamma_T(\mathbf{x}) \mathbf{w} + o(\delta)) \bigg) \\ &= \underbrace{\eta_{T-1} L_T(\mathbf{x}) + \lambda_{T-1} \nabla \log p_{T-1} (L_T(\mathbf{x}))}_{\text{recursion on the unperturbed data } \mathbf{x}} + \underbrace{\delta \eta_{T-1} \gamma_T(\mathbf{x}) \mathbf{w} + \delta \lambda_{T-1} H_{T-1} (L_T(\mathbf{x})) \gamma_T(\mathbf{x}) \mathbf{w}}_{\text{linear term}} \\ &+ \underbrace{o(\delta)}_{\text{lower order term}} \\ &= L_{T-1} \circ L_T(\mathbf{x}) + \delta \gamma_{T-1}(\mathbf{x}) \mathbf{w} + o(\delta). \end{split}$$

where

$$\gamma_{T-1}(\mathbf{x}) := (\eta_{T-1}I + \lambda_{T-1}H_{T-1}(L_T(\mathbf{x})))\gamma_T(\mathbf{x})$$

So we have

$$\mathbf{x}_0(\mathbf{x} + \delta \mathbf{w}, T) := L_0 \circ \cdots L_{T-1} \circ L_T(\mathbf{x}) + \delta \gamma_0(\mathbf{x}) \mathbf{w} + o(\delta)$$

Now let  $\lambda$  be the scale of the perturbation, such that  $\lambda > 0$  and  $\lambda \in \mathbb{R}$ , and let  $\Delta \mathbf{x}$  be the unit-length perturbation to the initial noise  $\mathbf{x}_T$ , we have:

$$\mathbf{x}_0(\mathbf{x}_T + \lambda \Delta \mathbf{x}, T) = \mathbf{x}_0(\mathbf{x}_T, T) + \lambda \gamma_0(\mathbf{x}_T) \Delta \mathbf{x} + o(\lambda)$$

We could continue applying  $L_{T-2}, L_{T-3}, \ldots, L_1$  on the above formula, and conclude:

$$\mathbf{x}_0(\mathbf{x}_T + \lambda \Delta \mathbf{x}, T) = x_0(\mathbf{x}_T) + \lambda \gamma_0(\mathbf{x}_T) \Delta \mathbf{x} + o(\lambda). \tag{5}$$

We might be particularly interested in the distance  $\|\mathbf{x}_0(\mathbf{x}_T + \lambda \Delta \mathbf{x}, T) - \mathbf{x}_0(\mathbf{x}_T, T)\|$ , our calculation directly implies:

$$\|\mathbf{x}_0(\mathbf{x}_T + \lambda \Delta \mathbf{x}, T) - \mathbf{x}_0(\mathbf{x}_T, T)\|_2 =$$

$$\|\lambda \gamma_0(\mathbf{x}_T) \Delta \mathbf{x}\|_2 + o(\lambda) = \lambda \|\gamma_0(\mathbf{x}_T) \Delta \mathbf{x}\|_2 + o(\lambda).$$
(6)

by applying triangle inequality twice:

$$\|\lambda \gamma_0(\mathbf{x}_T)\Delta \mathbf{x}\|_2 - \|o(\lambda)\|_2 \le \|\mathbf{x}_0(\mathbf{x}_T + \lambda \Delta \mathbf{x}, T) - \mathbf{x}_0(\mathbf{x}_T)\|_2 \le \|\lambda \gamma_0(\mathbf{x}_T)\Delta \mathbf{x}\|_2 + \|o(\lambda)\|_2$$

#### A.2 Proof in Section 3.3

We first state the detailed assumptions posed in Section 3.3. Define the function

$$h(t, \mathbf{y}) := -\frac{1}{2} \sqrt{\alpha(t)} \frac{\alpha'(t)}{\alpha_t^2} \nabla \log p_t \left( \frac{\mathbf{y}}{\sqrt{\sigma^2(t) + 1}} \right).$$

We assume this function has a continuous derivative (i.e.,  $C^1$ ) on the whole space  $[0,T] \times \mathbb{R}^m$ . Moreover, we assume there exists C(t) such that:

$$||h(t, \mathbf{y}) - h(t, \mathbf{x})||_2 \le C(t) ||\mathbf{y} - \mathbf{x}||_2$$

for every  $\mathbf{x}, \mathbf{y}, t$ , and  $\max_{t \in [0,T]} C(t) \leq C < \infty$ .

*Proof of Proposition 2.* We first show the ODE (4) exists a unique solution. We can rewrite the (4) as:

$$\begin{split} \mathrm{d}\bar{\mathbf{x}}_t &= -\sqrt{1-\alpha(t)}\nabla\log p_t\left(\frac{\bar{\mathbf{x}}_t}{\sqrt{\sigma^2(t)+1}}\right)\mathrm{d}\sigma(t) \\ &= -\sigma'(t)\sqrt{1-\alpha(t)}\nabla\log p_t\left(\frac{\bar{\mathbf{x}}_t}{\sqrt{\sigma^2(t)+1}}\right)\mathrm{d}t \\ &= -\frac{1}{2}\sqrt{\alpha(t)}\frac{\alpha'(t)}{\alpha_t^2}\nabla\log p_t\left(\frac{\bar{\mathbf{x}}_t}{\sqrt{\sigma^2(t)+1}}\right)\mathrm{d}t \quad \text{ as } \sigma(t) = \sqrt{(1-\alpha(t))/\alpha(t)} \\ &= h(t,\bar{\mathbf{x}}_t)\mathrm{d}t. \end{split}$$

Given  $h(t, \mathbf{y}) \in C^1$  and uniformly Lipschitz in  $\mathbf{y}$ , it follows from the Picard-Lindelöf Theorem (e.g., Theorem 1.1 of [19]) that our ODE (4) has a unique solution for any initialization  $\bar{\mathbf{x}}_T = \bar{\mathbf{x}}$ .

Next, it follows from Theorem 3.1 of [19] that the solution  $\bar{\mathbf{x}}_0(\bar{\mathbf{x}},T) \in C^1$ , i.e., the solution depends continuously and differentiably on its initialization  $\bar{\mathbf{x}}$ . Thus,

$$\bar{\mathbf{x}}_0(\mathbf{x}_T + \lambda \Delta \mathbf{x}, T) = \bar{\mathbf{x}}_0(\mathbf{x}_T, T) + \lambda J_{\bar{\mathbf{x}}}(\mathbf{x}_T) \Delta \mathbf{x} + o(\lambda),$$

where  $J_{\mathbf{x}}$  is the Jabobian matrix of the function  $\bar{\mathbf{x}}_0(\bar{\mathbf{x}},t)$  with respect to  $\bar{\mathbf{x}}$ . This concludes the proof of Proposition 2.

*Proof of Proposition 3.* Let  $\bar{\mathbf{x}}_T$  and  $\bar{\mathbf{x}}_T + \lambda \Delta \mathbf{x}$  be two fixed initializations. Define

$$\mathbf{y}_t := \bar{\mathbf{x}}_t(\bar{\mathbf{x}}_T) - \bar{\mathbf{x}}_t(\bar{\mathbf{x}}_T + \lambda \Delta \mathbf{x})$$

as the difference between the solutions of (4) at time  $t \in [0, T]$ .

Taking derivative on y with respect to t yields:

$$\mathbf{y}_t' = h(t, \bar{\mathbf{x}}_t(\bar{\mathbf{x}}_T)) - h(t, \bar{\mathbf{x}}_t(\bar{\mathbf{x}}_T + \lambda \Delta \mathbf{x})).$$

By the Lipschitz continuity:

$$\|\mathbf{y}_t'\|_2 \le C\|\bar{\mathbf{x}}_t(\bar{\mathbf{x}}_T) - \bar{\mathbf{x}}_t(\bar{\mathbf{x}}_T + \lambda \Delta \mathbf{x})\|_2 = C(t)\|\mathbf{y}_t\|_2$$

Denote  $\mathbf{y}_t$  by  $(\mathbf{y}_{1,t}, \mathbf{y}_{2,t}, \dots, \mathbf{y}_{m,t})^{\top}$ , we have:

$$\begin{split} \frac{\mathrm{d}\|\mathbf{y}_t\|_2}{\mathrm{d}t} &= \frac{\mathrm{d}\sqrt{\sum_{i=1}^m \mathbf{y}_{i,t}^2}}{\mathrm{d}t} \\ &= \frac{1}{2} \frac{\sum_{i=1}^m 2\mathbf{y}_{i,t}\mathbf{y}_{i,t}'}{\sqrt{\sum_{i=1}^m \mathbf{y}_{i,t}^2}} \\ &= \frac{\sum_{i=1}^m \mathbf{y}_{i,t}\mathbf{y}_{i,t}'}{\|\mathbf{y}_t\|_2} \\ &\leq \frac{\|\mathbf{y}_t\|_2 \|\mathbf{y}_t'\|_2}{\|\mathbf{y}_t\|_2} \qquad \text{Cauchy-Schwarz inequality} \\ &= \|\mathbf{y}_t'\|_2. \end{split}$$

Thererfore, we have

$$\frac{\mathrm{d}\|\mathbf{y}_t\|_2}{\mathrm{d}t} \le C(t)\|\mathbf{y}_t\|_2.$$

Applying Grönwall's inequality on the function  $\|\mathbf{y}_t\|$ , we have:

$$\|\mathbf{y}_t\|_2 \le \exp\left(\int_t^T C(t) dt\right) \|\lambda \Delta \mathbf{x}\|_2$$

for every  $0 \le t \le T$ . Taking t = 0, we have

$$\|\bar{\mathbf{x}}_0(\mathbf{x}_T + \lambda \Delta \mathbf{x}, T) - \bar{\mathbf{x}}_0(\mathbf{x}_T, T)\|_2 \le \exp\left(\int_0^T C(t) dt\right) |\lambda| \|\Delta \mathbf{x}\|_2.$$

as claimed in Proposition 3.

#### A.3 Proof in Section 4

Proof of Proposition 5. It is known

$$\mathbb{E}[\|\mathbf{x} + \Delta \mathbf{x}\|_{2}^{2}] = \|\mathbb{E}[\mathbf{x} + \Delta \mathbf{x}]\|_{2}^{2} + \operatorname{tr}(\operatorname{Cov}[\mathbf{x} + \Delta \mathbf{x}])$$
$$= \|\mathbf{x}\|_{2}^{2} + \operatorname{tr}(\operatorname{Cov}[\Delta \mathbf{x}])$$
$$\geq \|\mathbf{x}\|_{2}^{2}$$

The equality is taken if and only if  $\operatorname{tr}(\operatorname{Cov}[\Delta \mathbf{x}]) = \sum_i \operatorname{Var}[\Delta \mathbf{x}_i] = 0$ . This is equivalent to saying that all components of  $\Delta \mathbf{x}$  are deterministic. Therefore, almost surely,  $\Delta \mathbf{x} = \mathbb{E}[\Delta \mathbf{x}] = 0$ .

*Proof of Proposition 6.* Given a standard normal vector  $\epsilon$ , we claim the following holds:

$$\frac{\|\epsilon - \mathbf{x}_T\|_2^2}{d} = \frac{\|\epsilon\|_2^2}{d} + \frac{\|\mathbf{x}_T\|_2^2}{d} + \frac{-2\epsilon \cdot \mathbf{x}_T}{d} \to 2$$

in  $L^2$  as  $d \to \infty$ . To see this, notice the first term is

$$\frac{\sum_{i=1}^{d} \epsilon_i^2}{d}$$

which converges to 1 by the law of large numbers, since  $\mathbb{E}[\epsilon_i^2] = 1$ . The second term converges to 1 by our assumption. The last term converges to 0 in  $L^2$  as

$$\mathbb{E}\left[\left\|\frac{-2\epsilon \cdot \mathbf{x}_T}{d}\right\|^2\right] = \frac{4\mathbb{E}\left[\sum_i \mathbf{x}_{T,i}^2 \mathbb{E}\left[\epsilon_i^2\right]\right]}{d^2} = \frac{4(d+o(d))}{d^2} \to 0.$$

Therefore the distance  $\|\epsilon - \mathbf{x}_T\|_2$  converges to  $2\sqrt{d}$  as  $d \to \infty$ . Similarly we can show  $\theta(\epsilon, \mathbf{x}_T)$ , the angle between  $\epsilon$  and  $\mathbf{x}_T$  converges to  $\pi/2$  as  $d \to \infty$ . In other words,  $\epsilon$  is approximately orthogonal to  $\mathbf{x}_T$  when the dimension d is large.

Therefore, with probability 1-o(1), the angle  $\theta$  in Algorithm 1 is  $\pi/2 \pm o(1)$ , and  $\|\epsilon - \mathbf{x}_T\|_2/2\sqrt{d} = 1 \pm o(1)$  as  $d \to \infty$ . Fix any  $M \le (2-\delta)\sqrt{d}$ , since the spherical interpolation smoothly interpolate between  $\mathbf{x}_0$  and  $\epsilon$ , there exists a C satisfying Algorithm 1 with input C output  $\mathbf{x}_T'$  with distance M to  $\mathbf{x}_T$  with probability 1-o(1).

We can indeed find an explicit  $C_0$  with slightly weaker guarantees, set

$$C_0 = \cos^{-1}\left(1 - \frac{M^2}{2\|\mathbf{x}_t\|_2^2}\right).$$

Then with probability 1 - o(1),  $C_0 \in (0, \pi/2)$ , and

$$\left\| \frac{\sin(C_0)}{\sin(\theta)} \cdot \epsilon + \frac{\sin(\theta - C_0)}{\sin(\theta)} \cdot \mathbf{x}_T - \mathbf{x}_T \right\| \le \left\| \frac{\sin(C_0)}{\sin(\theta)} \cdot \epsilon + \frac{\sin(\theta - C_0)}{\sin(\theta)} \cdot \mathbf{x}_T - \sin(C_0)\epsilon - \sin(\theta - C_0)\mathbf{x}_T \right\| + \left\| \sin(C_0)\epsilon + \sin(\theta - C_0)\mathbf{x}_T - \mathbf{x}_T \right\|$$

by triangle's inequality. Meanwhile, the first term is  $o(\sqrt{d})$  as  $\sin(\theta) = \sin(\pi/2 + o(1)) = 1 + o(1)$  and  $\cos(\theta) = 1 - o(1)$ . The square of the second term is

$$\|\sin(C_0)\epsilon + \sin(\theta - C_0)\mathbf{x}_T - \mathbf{x}_T\|^2 = \sin(C_0)^2 \|\epsilon\|^2 + (1 - \sin(\theta - C_0))^2 \|\mathbf{x}_T\|^2 + 2\sin(C_0)(\sin(\theta - C_0) - 1)\epsilon \cdot \mathbf{x}_T$$
$$= \sin(C_0)^2 (d + o(1)) + (1 - \sin(\theta - C_0))^2 (d + o(1)) + o(d)$$

The last term is o(d) as  $\epsilon \cdot \mathbf{x}_T/d \to 0$  as we analyzed above. Using again  $\theta = \pi/2 + o(1)$ , we know  $\sin(\theta - C_0) = \sin(\pi/2 - C_0) + o(1) = \cos(C_0) + o(1)$ . Hence we clean the above equation:

$$\begin{aligned} \|\sin(C_0)\epsilon + \sin(\theta - C_0)\mathbf{x}_T - \mathbf{x}_T\|^2 &= d(\sin(C_0)^2 + (1 - \cos(C_0))^2) + o(d) \\ &= d(2 - 2\cos(C_0)) + o(d) \\ &= d\left(2 - 2 + \frac{M^2}{\|\mathbf{x}_t\|_2^2}\right) + o(d) \\ &= M^2 + o(d), \end{aligned}$$

where the last equality follows from  $\|\mathbf{x}_T\|_2^2 = d + o(1)$ . Finally, taking the square root and plugging back into the triangle inequality, we have:

$$\|\mathbf{x}_T' - \mathbf{x}_T\| = M + o(\sqrt{d}).$$

Proof of Proposition 7. We can write  $\mathbf{x} = r_0 \mathbf{x}_0$  where  $r_0 = ||\mathbf{x}||$  and  $\mathbf{x}_0 = \mathbf{x}/r_0$  belongs to  $S^{d-1}$ , the unit sphere in  $\mathbb{R}^d$ .

Meanwhile, it is well known that we can generate  $\epsilon \sim \mathbb{N}(0, I_d)$  via 1) sample  $r_1^2 \sim \chi^2(d)$  from the chi-squared distribution with parameter d, 2) sample  $\mathbf{u} \sim \mathrm{Unif}(S^{d-1})$  uniformly on the d-dim unit sphere, 3) set  $\epsilon = r_1 u$ . Therefore, let

$$\theta = \theta(\mathbf{u}) := \arccos\langle \mathbf{x}_0, \mathbf{u} \rangle$$
$$s(\theta) := \frac{\sin(c\theta)}{\sin \theta}$$
$$t(\theta) := \frac{\sin((1 - c)\theta)}{\sin \theta}.$$

We rewrite y as

$$\mathbf{y} = s(\theta)r_1\mathbf{u} + t(\theta)r_0\mathbf{x}_0$$

Now we calculate  $\mathbb{E}[\|\mathbf{y}\|^2]$ :

$$\mathbb{E}[\|\mathbf{y}\|^2] = \mathbb{E}[s(\theta)^2 r_1^2 \|\mathbf{u}\|^2] + \mathbb{E}[t(\theta)^2 r_0^2 \|\mathbf{x}_0\|^2] + \mathbb{E}[2r_0 r_1 s(\theta) t(\theta) \langle \mathbf{u}, \mathbf{x}_0 \rangle]$$

Our first claim is the cross term  $\mathbb{E}[2r_0r_1s(\theta)t(\theta)\langle\mathbf{u},\mathbf{x}_0\rangle]$  is zero. To see this, we first observe since  $r_1$  and  $\mathbf{u}$  are independent, we have

$$\mathbb{E}[2r_0r_1s(\theta)t(\theta)\langle\mathbf{u},\mathbf{x}_0\rangle] = 2r_0\mathbb{E}[r_1]\mathbb{E}[s(\theta)t(\theta)\langle\mathbf{u},\mathbf{x}_0\rangle]$$

We examine the expectation  $\mathbb{E}[s(\theta)t(\theta)\langle \mathbf{u}, \mathbf{x}_0\rangle]$  where the only random variable is the direction vector  $\mathbf{u}$ . Replacing  $\mathbf{u}$  with  $-\mathbf{u}$  sends the angle  $\theta$  to  $\pi - \theta$ , which will not change the value of  $s(\theta), t(\theta)$ . However, the inner product flips sign: $\langle -\mathbf{u}, \mathbf{x}_0 \rangle = -\langle \mathbf{u}, \mathbf{x}_0 \rangle$ . Consequently, the function of interest:

$$F(\mathbf{u}) := s(\theta(\mathbf{u}))t(\theta(\mathbf{u}))\langle u, \mathbf{x}_0 \rangle$$

is an odd function of u. Therefore,

$$\mathbb{E}_{\mathbf{u} \in \mathrm{Unif}(S^{d-1})}[s(\theta)t(\theta)\langle \mathbf{u}, \mathbf{x}_0 \rangle] = 0.$$

Now the expected distance simplifies to

$$\mathbb{E}[\|\mathbf{y}\|^{2}] = \mathbb{E}[s(\theta)^{2}r_{1}^{2}\|\mathbf{u}\|^{2}] + \mathbb{E}[t(\theta)^{2}r_{0}^{2}\|\mathbf{x}_{0}\|^{2}]$$
$$= d\mathbb{E}[s(\theta)^{2}] + r_{0}^{2}\mathbb{E}[t(\theta)^{2}]$$

The next observation is the following trigonometric identity:

$$s(\theta)^{2} + t(\theta)^{2} + 2s(\theta)t(\theta)\cos(\theta) = 1$$

for any  $c \in (0, 1), \theta \in (0, \pi)$ .

To show this identity, set  $\alpha = c\theta$ ,  $\beta = (1-c)\theta$ . Then  $s = \sin(\alpha)/\sin(\alpha+\beta)$ ,  $t = \sin(\beta)/\sin(\alpha+\beta)$ . The left hand side of the claimed identity equals

$$\frac{\sin^2(\alpha) + \sin^2(\beta) + 2\sin(\alpha)\sin(\beta)\cos(\alpha + \beta)}{\sin^2(\alpha + \beta)}$$

Now we expand  $\sin^2(\alpha + \beta)$  as

$$\begin{split} \sin^2(\alpha+\beta) &= (\sin(\alpha)\cos(\beta) + \cos(\alpha)\sin(\beta))^2 \\ &= \sin^2(\alpha)\cos^2(\beta) + \cos^2(\alpha)\sin^2(\beta) + 2\sin(\alpha)\cos(\alpha)\sin(\beta)\cos(\beta) \\ &= \sin^2(\alpha) - \sin^2(\alpha)\sin^2(\beta) + \sin^2(\beta) - \sin^2(\alpha)\sin^2(\beta) + 2\sin(\alpha)\cos(\alpha)\sin(\beta)\cos(\beta) \\ &= \sin^2(\alpha) + \sin^2(\beta) + 2\sin(\alpha)\sin(\beta)(\cos(\alpha)\cos(\beta) - \sin(\alpha)\sin(\beta)) \\ &= \sin^2(\alpha) + \sin^2(\beta) + 2\sin(\alpha)\sin(\beta)\cos(\alpha + \beta), \end{split}$$

as claimed.

Leveraging this equality  $s(\theta)^2 + t(\theta)^2 + 2s(\theta)t(\theta)\cos(\theta) = 1$  and taking expectation with respect to  $\mathbf{u}$  implies:

$$\mathbb{E}[s(\theta)^2] + \mathbb{E}[t(\theta)^2] = 1,$$

as the cross term is zero as proved before.

Now let  $s_c := \mathbb{E}[s(\theta)^2] \in (0,1)$ , we have

$$\mathbb{E}[\|\mathbf{y}\|^2] = ds_c + r_0^2 (1 - s_c)$$

Therefore

$$\delta(\mathbf{y}) = |\mathbb{E}[\|\mathbf{y}\|^2] - d| = (1 - s_c)|d - r_0^2| = (1 - s_c)|\|\mathbf{x}\|^2 - d| \le |\|\mathbf{x}\|^2 - d| = \delta(\mathbf{x})$$

# A.4 Why linear interpolation fails

To further support this point, we provide additional theoretical analysis to justify why simple linear interpolation does not work well for sampling. Formally, let  $\|\Delta x\|_2 = \|x\|_2$ , and its direction is uniformly distributed, and  $\mathbb{E}[\Delta x] = 0$ . For  $0 < \alpha < 1$ , we have:

$$\mathbb{E}\left[\|\alpha x + (1 - \alpha)\Delta x\|_2^2\right] < \|x\|_2^2$$

**Proof.** We have:

$$\|\alpha x + (1 - \alpha)\Delta x\|_2^2 = \alpha^2 \|x\|_2^2 + 2\alpha(1 - \alpha)(x \cdot \Delta x) + (1 - \alpha)^2 \|\Delta x\|_2^2$$

Since 
$$\mathbb{E}\left[\alpha(1-\alpha)(x\cdot\Delta x)\right]=\alpha(1-\alpha)x\cdot\mathbb{E}[\Delta x]=0$$
, we have: 
$$\mathbb{E}\left[\|\alpha x+(1-\alpha)\Delta x\|_2^2\right]=\alpha^2\|x\|_2^2+(1-\alpha)^2\|\Delta x\|_2^2=(\alpha^2+(1-\alpha)^2)\|x\|_2^2$$

Since  $2\alpha(\alpha-1) < 0$ , we have  $(\alpha^2 + (1-\alpha)^2) < 1$ , and we can conclude that using simple linear interpolation cannot preserve the norm, leading to falling apart from the Gaussian sphere.

# **B** More Analysis on Linearity

# **B.1** Validation of Linearity Phenomenon on changing $C_0$

**Experimental setting.** We perform extensive experiments on both pixel diffusion models on the FFHQ and CIFAR-10 dataset and latent diffusion models on the Celeba-HQ and fMoW dataset. For each experiment, we first sample 50 images as target images from each validation dataset from FFHQ [22], CIFAR-10[25], and Celeba-HQ [43]. We also pick one images each class from the validation set of the fMoW dataset [5] for further verification. Then for the FFHQ and CIFAR-10 selected data, we use pixel diffusion models as backbone; for Celeba-HQ and fMoW we use stable diffusion 1.5 as the backbone. The prompt for Celeba-HQ is given by "A high quality photo of a face" and the prompt for fMoW is given by "satellite images". Then, we use each image as a target mean and perform CCS sampling as in Alg.1.

For each target image, we sample eight  $C_0$  from a uniform [0, 0.9] distribution. For each  $C_0$ , we sample 24 images. Then we compute the average  $L^2$  distance between the sampled images and the target mean for each scale.

**Evaluations.** To quantitatively evaluate the linearity phenomenon, we compute the R-square between the input perturbation scales and the normalized average residual norms (scale between 0-1) for 4 datasets with both pixel diffusion models and latent diffusion models. Note that since different target means can lead to different slopes by different Hessian matrices, we normalize the residual norms. Specifically, we compute empirical slope a and bias b between  $x = \sin(C_0)$  and  $y = \mathbb{E}[\|\mathbf{x}_0' - \mathbf{x}_0\|_2]$  each target mean, and then normalize the average  $L^2$  distance to be:  $y' = \frac{y-b}{a}$ .

**Results.** We observe a very strong linearity in the above experiments. Especially for pixel diffusion models, the R-square exceeds 0.98 for both datasets, which indicates almost a perfect linear relationship. For latent diffusion models, the linearity is slightly weaker, but still above 0.94 in R-square for both datasets. This is expected since Stable Diffusion use a nonlinear autoencoder and trained on a different dataset. We also present more quantitative results in Fig. 2 and qualitative results in Fig. 1. Surprisingly, we also observe a very linear semantic change in additional to pixel-value change.

Pixel Diffusion Models		Latent Diffusion Models		
FFHQ	CIFAR-10	CelebA-HQ	fMoW	
0.995	0.988	0.959	0.947	

Table 4: R-square between scales of input perturbation and normalized residual norms

### **B.2** Validation of Compositional Linearity

**Experimental setting.** Here we just have motivation similar to the previous one. We first sample a random noise  $\epsilon_0 \in N(0,I)$ , and then another random noise  $\epsilon_1 \in N(0,I)$ . We perform spherical interpolation on  $\epsilon_0$  and  $\epsilon_1$ , and inference using a joint noise. We can adjust  $C_0$  to decrease the strength of sspherical interpolation to preserve orignal image structure. This. We sample  $C_0$  uniformly and continue sample  $\epsilon_0$  and  $\epsilon_1$  for evaluation. Then we compare the cosine distance between  $\mathrm{DDIM}(slerp(\epsilon_0,\epsilon_1,C_0))$  and  $a\mathrm{DDIM}(\epsilon_0)+b\mathrm{DDIM}(\epsilon_1)$ , where a and b are given by  $slerp(\epsilon_0,\epsilon_1,C_0)$ . We still find very large linearity, and the linearity decreases for Latent Diffusion Models. The quantitative results using four datasets, each with 100 evaluations are attached below in Table 5:

Pixel Diffusion Models		Latent Diffusion Models	
FFHQ	CIFAR-10	CelebA-HQ	fMoW
0.958	0.942	0.901	0.920

Table 5: Cosine similarity between samples generated by spherical interpolated initial noise, and linear combination of samples.

#### **B.3** Mathematical Explanation of the Linearity

**Bound the Linear Approximation Error of Score Function** 

Let

$$z = \sqrt{\delta}x_0 + \sqrt{1 - \delta} \, \epsilon, \quad f(x) = \text{data distribution}$$

$$\nu_\delta(x) = f\left(\frac{x}{\sqrt{\delta}}\right) \cdot \frac{1}{\sqrt{\delta}}, \quad u(x) = \mathcal{N}(0, 1 - \delta)$$

Then the density of z is:

$$f_z(z) = (\nu * u)(z)$$

#### Score Function and Its Derivatives

The score function is:

$$\nabla \log f_z(z) = \frac{\mathbb{E}_{u(x)}[\nabla \nu(z+x)]}{\mathbb{E}_{u(x)}[\nu(z+x)]}$$

Let:

$$A(z) := \mathbb{E}_{u(x)}[\nu(z+x)], \quad B(z) := \mathbb{E}_{u(x)}[\nabla \nu(z+x)], \quad C(z) := \mathbb{E}_{u(x)}[\nabla^2 \nu(z+x)]$$

Then the second derivative is:

$$\nabla^2 \log f_z(z) = \frac{C(z)}{A(z)} - \frac{B(z)B(z)^{\top}}{A(z)^2}$$

Assuming  $\nabla A(z) = B(z)$ ,  $\nabla B(z) = C(z)$ , and  $\nabla C(z)$  exists, the third derivative becomes:

$$\nabla^3 \log f_z(z) = \frac{\nabla C(z)}{A(z)} - \frac{C(z) \otimes B(z)}{A(z)^2} - \frac{C(z)B(z)^\top + B(z) \otimes C(z)}{A(z)^2} + \frac{2B(z)B(z)^\top \otimes B(z)}{A(z)^3}$$

#### Norm Bound on the Third Derivative

Suppose:

$$||C(z)||_2 \le c$$
,  $||B(z)||_2 \le b$ ,  $A(z) \ge a > 0$ ,  $||\nabla C(z)||_2 \le d$ 

Then:

$$\|\nabla^3 \log f_z(z)\|_2 \le \frac{d}{a} + \frac{3bc}{a^2} + \frac{2b^3}{a^3}$$

#### **Taylor Approximation and Linearization Error Bound**

Let  $z_0$  be a reference point. Then the second-order Taylor expansion of the score function is:

$$\nabla \log f_z(z) \approx \nabla \log f_z(z_0) + \nabla^2 \log f_z(z_0)(z-z_0)$$

The remainder (linearization error) satisfies:

$$\|\nabla \log f_z(z) - \nabla \log f_z(z_0) - \nabla^2 \log f_z(z_0)(z - z_0)\|_2 \le \frac{1}{2} \sup_{t \in [0,1]} \|\nabla^3 \log f_z(z_0 + t(z - z_0))\|_2 \cdot \|z - z_0\|_2^2$$

Using the third derivative bound, we get the formula for linear approximation error bound:

$$\|\mathcal{E}(z, z_0)\|_2 \le \frac{1}{2} \left( \frac{d}{a} + \frac{3bc}{a^2} + \frac{2b^3}{a^3} \right) \cdot \|z - z_0\|_2^2$$

By this bound, we may argue that the probability density of the sampling center, the curvature and gradient of the distribution (smoothness) impact the linearity error the most. If we are in the high probability region (a local maximum), assume that the curvature of probability distribution at that place is small, we will have low linear approximation error. So more complicated dataset may have less linearity since it is more likely to have discontinuous regions or low-density regions. This mathematical derivation explains the decrease of linearity from Pixel diffusion models to LDMs as shown in Table: 5.

#### **B.4** Linearity Analysis for OOD and Multimodal data

To further investigate this relationship, we perform additional experiments on three more datasets to test how the linearity changes for multimodal distributions. We are interested in:

- 1. How is the linearity when the model is trained on a multimodal dataset and samples an out-of-distribution target image from another highly multimodal dataset, or an OOD simple dataset?
- 2. How is the linearity when the model is trained on a simple dataset (for example, FFHQ) and samples on an out-of-distribution multimodal dataset, or an OOD simple dataset?
- 3. How is the linearity when training on a simple dataset and sampling on the same dataset?
- 4. How is the linearity comparing model trained on multimodal dataset in-distribution and model trained on simple dataset testing in-distribution?

In our experiment section of the paper, we cover partially 1, 3, and 4. We test pixel diffusion models on FFHQ and CIFAR datasets. We also test the Stable Diffusion model (1.5) trained on a complex dataset (LAION-5B) on the human face dataset (CelebA-HQ). We observe that diffusion models trained on simple datasets (FFHQ) and tested on distributions exhibiting significant differences show stronger linearity than Stable Diffusion trained on CelebA-HQ.

We observed in our paper that linearity decreases slightly when comparing diffusion models trained on multimodal datasets to diffusion models with simple training data. CIFAR-10, being a dataset with different classes, shows a slightly lower linearity score compared to FFHQ even though CIFAR-10 is lower resolution. Empirically, we observe sudden changes of image semantics occasionally.

- 1. We pick 4 images from classes 0, 4, ..., 99 from the validation set of ImageNet.
- 2. We pick five videos from classes: "Applying Eye Makeup", "Baby Crawling", "Billiard", and "Blow Dry Hair" from the UCF-101 dataset, and sample five frames per video.
- 3. We pick 10 images from each organ site in the AAPM dataset, which consists of CT scans of different body parts. These datasets are different from the training data of SD1.5.

We use the same linearity testing methods as in Section 5.1 of our main paper (and also in Appendix B). We first summarize the results for Stable Diffusion 1.5:

Dataset	ImageNet	UCF-101	CelebA-HQ	fMoW
$R^2$	0.960	0.962	0.959	0.947
Cosine similarity of linear combinations	0.922	0.924	0.901	0.920

Table 6: Linearity statistics across multimodal datasets for Stable Diffusion 1.5.

The results show that for multimodal datasets (containing many classes like ImageNet or UCF-101), there is no evidence of a decrease in linearity compared to simple datasets (CelebA-HQ). For the same backbone model trained on a large multimodal dataset (LAION-5B), the slightly lower linearity on CelebA-HQ may be due to data processing techniques such as upscaling, which introduces blurriness and removes latent noise patterns from the Gaussian sphere.

When testing the linearity on OOD datasets for models trained on simple datasets, we observe a significant linearity drop. We compare models trained on multimodal data and tested on simple datasets. Results are computed using the same testing method as before and as described in Appendix B. Here, "trained  $\rightarrow$  tested" means that the model is trained on the training set of the "trained" dataset and tested on the validation set of "tested".

For fair evaluation, we use the same model architecture (DDPM++) with the same training loss for these two pixel-space diffusion models. We find that for non-foundation models, OOD linearity drops significantly. The multimodal backbone has a slightly lower linearity score than the simple data backbone due to complexity in its training data (it trains on LAION-5B). The probability distribution of multimodal images plays an important role in linearity.

$\textbf{Dataset (trained} \rightarrow \textbf{tested)}$	$\textbf{ImageNet} \rightarrow \textbf{FFHQ}$	$\mathbf{FFHQ} \to \mathbf{ImageNet}$	$\overline{\textbf{FFHQ}} \to \overline{\textbf{FFHQ}}$
$R^2$ Cosine Similarity	0.934	0.938	0.995
	0.902	0.905	0.958

Table 7: Cross-dataset linearity comparison between multimodal and simple dataset training/testing. Results are computed using the same testing method as before and as described in Appendix B. Here, "trained  $\rightarrow$  tested" means that the model is trained on the training set of the "trained" dataset and tested on the validation set of "tested".

#### C Limitations and Clarifications

# C.1 DDIM inversion not conforming to standard Gaussian distribution.

- 1. Investigation of Sample Quality Drop. To investigate whether there is a sample quality drop, we use our CelebA-HQ validation set for additional experiments. This dataset is originally of size  $256 \times 256$ , and we upscale it to  $512 \times 512$ , so it becomes slightly blurry and sometimes gives inversions not perfectly on the sphere. We partition the CelebA-HQ data into two sets:
  - Not STG noise: encoded noise with mean deviation > 0.03 or std deviation > 0.03 from standard Gaussian distribution.
  - STG noise: all remaining samples.

We compute performance metrics of these images on Stable Diffusion with rMSE target 0.07. The results are summarized below:

Set	PSNR ↑	<b>MUSIQ</b> ↑	CLIP-IQA↑	SD↑
Not STG noise	30.86	49.43	0.734	0.053
STG noise	30.10	49.74	0.731	0.054

Table 8: Comparison of image quality for STG vs. non-STG noise at rMSE target 0.07 on CelebA-HQ.

We do not find significant image quality differences between these two sets. Indeed, after our CCS interpolation at the 0.07 rMSE target, the interpolated noise of the non-STG noise group all falls within 0.01 difference between zero mean and unit standard deviation. Empirically, at low rMSE levels, the noise may be non-standard Gaussian, but the samples remain close to the input image. At higher rMSE levels, the interpolated noise becomes more standard Gaussian, resulting in good image quality.

**2. Verification of Gaussianity with Interpolation Strength.** To verify that the Gaussian distribution becomes more standard with stronger interpolation, we compute the average deviation of mean (from 0) and deviation of variance (from 1) for the CelebA-HQ experiment. We find that as the interpolation strength  $C_0$  increases, the deviation quickly narrows:

$C_0$	Deviation in mean	Deviation in std
0.0	0.025	0.023
0.2	0.013	0.016
0.3	0.011	0.009
0.4	0.010	0.008
0.5	0.009	0.006
0.6	0.007	0.005

Table 9: Deviation of mean and standard deviation across interpolation strength  $C_0$  in CelebA-HQ experiments.

**3. Discussion.** In our paper,  $C_0$  is mostly between 0.3 and 0.6, so we do not worry much about the interpolated noise being non-standard Gaussian. We also conduct experiments at different rMSE target levels (with varying  $C_0$ ) and observe that increasing interpolation strength may lead to slightly better image quality when the input image is not very good.

#### C.2 Some other common confusions

There might be some misunderstanding of our method and experiments. To clarify:

- the baseline CCDF is just a special type of SDEdit.
- Our method **does not** specifically focus on improving quality in our main experiments in the main paper (the improvement in sample quality is a very nice add-on). Instead, it focuses on controllability (how to sample around a mean with a target MSE). So even though our performance gain is not that large, we achieve much better controllability over the edit strength which is measured as the distance between sample mean and the real input image (as demonstrated in Fig. 3).

# **D** Additional Results and Experiments

In this section, we clarify some implementation details, providing more details on algorithms and visualization. We also provide more quantitative results and computational efficiency analysis.

# D.1 More Details on Controllable Sampling

**Experimental Set up** For pixel diffusion models, we use the first 50 images from the validation data from the FFHQ-256 [6] dataset. Then we set each image as the target mean and then sample 120 images (6000 images in total) with each target mean with a target rMSE (square root of average L-2 norm of the residuals between the sample and target mean) of 0.12. Then we test on the CIFAR-10 dataset. We randomly sample 20 images serving as target means, and then sample 120 images for each target mean with a target rMSE level of 0.11.

For Stable Diffusion, we use the SD1.5 checkpoint [31]. We study a more challenging scenario (degraded low-resolution input images with conditional text-guided latent diffusion model). We sample 50 images from the validation set from Celeba-HQ dataset with resolution  $256 \times 256$ , and then use bicubic upsampling to upscale it to  $512 \times 512$ . Note that SD1.5 is not trained on the Celeba-HQ dataset so this demonstrates the generalization capability of algorithms. We use the same prompt and CFG level in the linearity control experiments.

#### **Implementation Detail**

We follow Alg. 1 in implementing our methods for pixel diffusion models, and Alg. 3 for latent diffusion models. We take the pretrained models for FFHQ and CIFAR-10 from the improved/guided diffusion repos [30, 13] for the pixel diffusion experiments, and the Stable Diffusion 1.5 [31] for latent diffusion experiments. For LDMs, we set  $t_0=45$ , where T=50 due to DDIM inversion performing worse with classifier-free guidance than unconditional models. We set the rMSE target to be 0.12, 0.11 for FFHQ and CIFAR-10 respectively, and 0.07 for Stable Diffusion experiments to test diverse control targets. The tolerance is set to be 0.01 in all cases. More details in the Appendix.

**Baselines** Since we are doing a novel task, we self-design the baselines with our proposed controller algorithm as an add-on.

- Gaussian Perturbation with Controller (GP-C): We add a Gaussian perturbation to the initial noisy image  $x_{t0}$ , where the perturbation scale is determined by our controller. This method resembles works that perform local editing [2].
- (Latent) Diffusion Posterior Sampling [6, 34] with controller (DPS-C): We perform posterior sampling with  $x_0$  as the measurement. The scale of the gradient term in (L)DPS can control the randomness, so we design a controller based on this. Details in the Appendix.
- ILVR with controller (ILVR-C): the ILVR algorithm [4] is for sampling high quality images based on a reference image. The larger the downsampling parameter gives a better diversity, we dynamically adjust that parameter as by our controller algorithm. Since it is designed only for DDPM, we do not experiment it with LDMs. Details in the Appendix.

- Come-closer-diffuse-faster with controller (CCDF-C): CCDF use DDPM forward to find a starting noise at  $t_0$ , and then perform reverse sampling based on that noise [8]. We adjust  $t_0$  based on our controller algorithm.
- Linear Interpolation with controller (LP-C): Replacing CCS spherical interpolation with linear interpolation

#### **Evaluation Metrics**

We first compute pixel-wise metrics to validate our hypothesis that sample mean is close to the target mean.

- PSNR (Peak Signal-to-Noise Ratio): quantifies the pixel-wise difference between the target mean and the sample mean.
- SD: the average of standard deviations of pixel intensities for each sampled image, which is used to measure the diversity of images.

Then we compute perceptual and reference-free metrics to measure the sample quality:

- MUSIQ [23]: measures the perceptual image quality, which focuses on low-level perceptual quality and is sensitive to blurs/noise/other distortions
- CLIP-IQA [40]: measures the semantic image quality, which is more higher-level than MUSIO
- Inception Score (IS) [32]: is used in the CIFAR-10 dataset to further measure image quality and diversity. Since CIFAR-10 has a low resolution and images are blurry, we report IS score instead of MUSIQ and CLIP-IQA for CIFAR-10.

Additionally, we compute LPIPS between sampled image and target mean, this reflects how the samples are preserving source information even though the MSE of those samples are controlled for a fair comparison.

#### Results

We observe that our method achieves preserving more source information while generate superior quality images with sufficient diversity. The Table below shows our superior performance in this direction:

Table 10: Performance with Stable Diffusion with MSE level 0.07

Methods	<b>PSNR</b> ↑	<b>LPIPS</b> ↓
GP-C	23.02	0.306
LDPS-C	24.56	0.351
CCDF-C	27.66	0.318
LP-C	29.59	0.322
CCS (Ours)-C	30.29	0.252

Table 11: Performance with Pixel Diffusion on FFHQ with MSE level 0.12

PSNR ↑	<b>LPIPS</b> ↓
18.88	0.596
20.04	0.443
21.02	0.459
23.52	0.461
23.41	0.489
25.13	0.332
	20.04 21.02 23.52 23.41

Table 12: Performance with Pixel Diffusion on CIFAR-10 with MSE level 0.11

Methods	PSNR ↑	LPIPS \
GP-C	24.66	0.409
DPS-C	23.13	0.567
CCDF-C	24.63	0.529
CCS (Ours)-C	26.05	0.328

# **D.2** Sampling Efficiency

We provide sampling speed and sampling NFE results in the table below. The sampling procedure consists of two steps:

- 1. **Controller tuning for statistical constraint.** This only needs to be performed once for each album. For our method and GP, we have an additional one-time single-image inversion step (which turns out to be very fast).
- 2. **Sampling with the tuned parameters.** Thanks to the linearity property, the binary search algorithm can efficiently find the feasible scale of perturbation, achieving the best controller tuning efficiency. Otherwise, the feasible scales may lie in a narrower region due to abrupt output changes or variability among samples, requiring more search rounds. We will include a detailed discussion of sampling efficiency in our revision.

We provide inference time for sampling 120 images around a target mean (with a tuning batch of size 20) for different methods below, using Stable Diffusion tested on one A40 GPU. The table reports the controller tuning NFE per batch, and sampling NFE per batch for each baseline.

Method	Sample time / image	<b>Controller Tuning NFE</b>	Sampling NFE
GP-C	1.66s	96	45
CCDF-C	1.73s	163	42
LDPS-C	5.84s	234	50
CCS-C (Ours)	1.65s	94	45

Table 13: Sampling efficiency comparison on Stable Diffusion tested on one A40 GPU.

The advantage of CCDF-C (or in other words, SDEdit-C) is that it does not require DDIM inversion, and requires fewer timesteps for denoising. However, it needs more controller tuning rounds since the outputs can be highly sensitive to some timesteps.

# D.3 More Results on Adjusting rMSE Control Levels

We perform additional experiments with sampling quality benchmarks using rMSE targets from [0.05, 0.06, 0.07, 0.08, 0.09, 0.10] for Stable Diffusion on CelebA-HQ. We observe that our method consistently performs quite well (PSNR is for sample mean vs. target image, SD is for diversity). Numbers are reported in the order of CCS-C / CCDF-C (the stronger/best baseline).

Target rMSE	PSNR ↑	<b>MUSIQ</b> ↑	<b>CLIP-IQA</b> ↑	SD ↑
0.05	32.22/30.86	49.60/49.53	0.729/0.730	0.036/0.034
0.06	31.44/29.03	49.58/49.02	0.731/0.731	0.043/0.040
0.07	30.29/27.66	49.66/48.91	0.732/0.735	0.053/0.051
0.08	30.10/26.80	49.85/48.23	0.742/0.729	0.056/0.052
0.09	29.74/25.98	49.82/48.01	0.740/0.732	0.061/0.054
0.10	29.31/25.20	49.80/46.74	0.731/0.727	0.063/0.057

Table 14: Sampling quality comparison for different rMSE targets on CelebA-HQ of CCS-C v.s. CCDF-C: CCS on the left, CCDF on the right

We also perform experiments on the FFHQ dataset for rMSE levels of [0.09, 0.12, 0.15], summarized below:

Target rMSE	PSNR ↑	<b>MUSIQ</b> ↑	CLIP-IQA ↑	SD↑
0.09	28.25/27.08	66.53/66.10	0.749/0.750	0.078/0.069
0.12	25.13/23.52	66.79/66.15	0.750/0.746	0.104/0.088
0.15	23.45/20.64	66.71/65.24	0.743/0.740	0.131/0.104

Table 15: Sampling quality results on FFHQ for different rMSE levels FOR CCS-C v.s. CCDF-C: CCS on the left, CCDF on the right

#### **Observations**

We observe several interesting phenomena in these additional experiments:

- 1. With more perturbation of noise (i.e., sample images farther from the target image), there is no decrease in sampling quality. Instead, there is a slight **increase in MUSIQ** for stable diffusion, meaning the image quality increases and looks sharper. One explanation is that the target image may not have good image quality or that the DDIM inversion is slightly apart from the Gaussian sphere. As the perturbation level increases, more Gaussian noise is interpolated, making the interpolated noise more "Gaussian" and improving image quality. Since Stable Diffusion is conditional and the input image is not from its training distribution, the DDIM inversion lies slightly off the Gaussian sphere. For FFHQ, however, the inversion is quite Gaussian, so there is no significant change in sample quality.
- 2. The sampled mean remains close to the target image as the rMSE level increases. We do not observe a sudden drop in controllability or diversity (PSNR and SD). However, with increasing rMSE targets, it becomes harder to control the sample mean close to the target mean, as demonstrated by declining PSNR. Nevertheless, this trade-off brings diversity improvement.

# D.4 More Details on improving sample quality.

Based on the observation that interpolates with a Gaussian make a non-Gaussian random variable more Gaussian, previous work points out that this gives a higher likelihood [30]. Hence, we propose to apply P-CCS on every step of reverse sampling with a very small interpolation factor. The algorithm is stated at Alg. 5. We observe significant gain in sample quality when testing on T2IBench [21]. Table. 16 shows the quantitative performance.

Table 16: Image Quality Scores for with and without P-CCS purified on T2IBench

Metric	With	Without
MUSIQ Score CLIP-IOA Score	55.499 0.541	52.951 0.530
CLII -IQA SCOIC	0.541	0.550

# **D.5** More Algorithms

We describe more details for the proposed P-CCS (Partial inversion CCS sampling) algorithms for different applications including constrained sampling, precise image editing and improving sampling quality.

Alg. 3 demonstrates using P-CCS for constrained sampling based on Stable Diffusion.

Alg. 4 demonstrates using P-CCS for precise image editing based on Stable Diffusion.

Alg. 5 demonstrates using P-CCS for improving the sample quality, instead of controllability.

# Algorithm 3 P-CCS for Constrained Sampling

**Requires:** target mean  $x_0$ , perturbation scale  $C_0$ , inversion time steps  $t_0$ , Encoder  $\mathcal{E}$  and Decoder  $\mathcal{D}$ ,

**Step 0:** Compute  $\mathbf{z}_0 = \mathcal{E}(x_0)$ , then compute the DDIM inversion of  $\mathbf{z}_0$ , i.e.  $\mathbf{z}_T =$  $\begin{array}{l} \text{DDIM}^{-1}(\mathbf{z}_0,0,t_0,c) \\ \textbf{Step 1:} \text{ Compute the noise from } \mathbf{z}_{t_0}, \text{by } \underline{\epsilon_{t_0}} = \mathbf{z}_{t_0} - \sqrt{\alpha_{t_0}} \cdot \mathbf{z}_0 \end{array}$ 

**Step 2:** Sample noise  $\epsilon \sim \mathbb{N}(0, 1 - \alpha_t)$ . Then compute

$$\theta = \cos^{-1} \left( \frac{\epsilon \cdot \epsilon_{target}}{||\epsilon||_2 ||\epsilon_{target}||_2} \right)$$

# Step 3:

Compute  $\epsilon'_{t_0}$  using spherical interpolation formula:

$$\epsilon'_{t_0} = \frac{\sin(C_0)}{\sin(\theta)} \cdot \epsilon + \frac{\sin(\theta - C_0)}{\sin(\theta)} \cdot \epsilon_{t_0}$$

Step 4: Compute  $\mathbf{z}'_{t_0} = \sqrt{\alpha_{t_0}} \cdot \mathbf{z}_0 + \epsilon'_{t_0}$ Step 5: Output sample  $\mathbf{x}'_0 = \mathcal{D}(\mathbf{z}'_0) = D(\mathrm{DDIM}(\mathbf{z}'_{t_0}, t_0, 0, c))$ 

# **Algorithm 4** P-CCS for Precise Image Editing

**Requires:** target mean  $x_0$ , perturbation scale  $C_0$ , inversion time steps  $t_0$ , Encoder  $\mathcal{E}$  and Decoder  $\mathcal{D}$ , source prompt  $c_s$ , target prompt  $c_t$ .

**Step 0:** Compute  $\mathbf{z}_0 = \mathcal{E}(x_0)$ , then compute the DDIM inversion of  $\mathbf{z}_0$  with the source prompt, i.e.  $\mathbf{z}_{t_0,s} = \text{DDIM}^{-1}(\mathbf{z}_0,0,t_0,c_s)$ , and the DDIM inversion with the target prompt, i.e.  $\mathbf{z}_{t_0,t} = \text{DDIM}^{-1}(\mathbf{z}_0,0,t_0,c_t)$ 

**Step 1:** Compute the noise from  $\mathbf{z}_{t_0,s}$ , by  $\epsilon_{t_0,s} = \mathbf{z}_{t_0,s} - \sqrt{\alpha_{t_0}} \cdot \mathbf{z}_0$ **Step 2:** Compute the noise from  $\mathbf{z}_{t_0,t}$ , by  $\epsilon_{t_0,t} = \mathbf{z}_{t_0,t} - \sqrt{\alpha_{t_0}} \cdot \mathbf{z}_0$ 

Step 3: Compute

$$\theta = \cos^{-1} \left( \frac{\epsilon_{t_0,s} \cdot \epsilon_{t_0,t}}{||\epsilon_{t_0,s}||_2 ||\epsilon_{t_0,t}||_2} \right)$$

#### Step 3:

Compute  $\epsilon'_{t_0}$  using spherical interpolation formula:

$$\epsilon'_{t_0} = \frac{\sin(C_0)}{\sin(\theta)} \cdot \epsilon_{t_0,s} + \frac{\sin(\theta - C_0)}{\sin(\theta)} \cdot \epsilon_{t_0,c}$$

Step 4: Compute  $\mathbf{z}'_{t_0} = \sqrt{\alpha_{t_0}} \cdot \mathbf{z}_0 + \epsilon'_{t_0}$ Step 5: Output sample  $\mathbf{x}'_0 = \mathcal{D}(\mathbf{z}'_0) = D(\mathrm{DDIM}(\mathbf{z}'_{t_0}, t_0, 0, c_t))$ , which is the precisely edited image with strength given by  $C_0$ .

# **More Figures**

Fig. 6 demonstrates the generated personalized album for CCS. Fig. 7 demonstrates example of applying P-CCS with SD1.5 on the Celeba-HQ dataset, we demonstrate that our algorithm can work well on in-the-wild images which are very different from the training.

Fig. 10 demonstrates the linear trend for each target mean on the FFHQ dataset.

Fig. 8,9 demonstrates an example of image editing controlled sampling with Alg. 4.

Fig. 11 demonstrates the linearity drop with OOD data.

# **Algorithm 5** P-CCS for Improving Sampling Quality

**Requires:** target mean  $x_0$ , perturbation scale  $C_0$ , inversion time steps  $t_0$ , Encoder  $\mathcal{E}$  and Decoder  $\mathcal{D}$ , condition c.

Step 0: Start by computing  $\mathbf{z}_0 = \mathcal{E}(x_0)$ , then compute the DDIM inversion of  $\mathbf{z}_0$  with the condition,

i.e.  $\mathbf{z}_{t_0} = \mathrm{DDIM}^{-1}(\mathbf{z}_0, 0, t_0, c),$ While  $t_0 > 0$ : Step 1: Compute the noise from  $\mathbf{z}_{t_0}$ , by  $\epsilon_{t_0} = \mathbf{z}_{t_0} - \sqrt{\alpha_{t_0}} \cdot \hat{\mathbf{z}_0}(z_T)$  using Tweedie's formula to compute  $\hat{\mathbf{z}}_0(z_T)$ .

**Step 2:** Sample a noise  $\epsilon \in N(0, 1 - \alpha_t)$ .

**Step 3:** Compute

$$\theta = \cos^{-1} \left( \frac{\epsilon_{t_0} \cdot \epsilon}{||\epsilon_{t_0}||_2 ||\epsilon||_2} \right)$$

Compute  $\epsilon'_{t_0}$  using spherical interpolation formula:

$$\epsilon'_{t_0} = \frac{\sin(C_0)}{\sin(\theta)} \cdot \epsilon_{t_0} + \frac{\sin(\theta - C_0)}{\sin(\theta)} \cdot \epsilon$$

Step 4: Compute  $\mathbf{z}'_{t_0} = \sqrt{\alpha_{t_0}} \cdot \mathbf{z}_0 + \epsilon'_{t_0}$ Step 5: Reverse Sampling using DDIM formula, and the modified  $\mathbf{z}_{t_0}$ ,  $t_0 = t_0 - 1$ 

**End While** 

**Step 6:** Output sample  $\mathbf{x}_0' = \mathcal{D}(\mathbf{z}_0') = D(\text{DDIM}(\mathbf{z}_{t_0}', t_0, 0, c_t))$ , which is the purified (improved) image with purification strength given by  $C_0$ .



Figure 6: a demo of sampled album with CCS algorithm on FFHQ dataset. Note that the sample mean is almost the same as the input image.

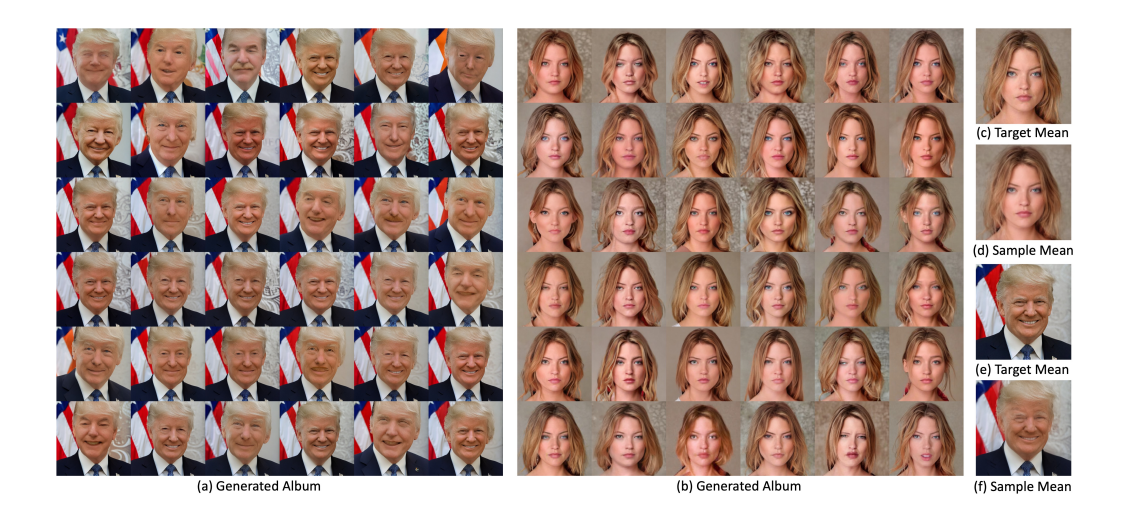


Figure 7: CCS-CT Sampled Images with Stable Diffusion 1.5. (a) Samples with an in-the-wild target mean (e) and a target rMSE 0.09; (b) Samples with a target mean (d) from Celeba-HQ dataset and a target rMSE 0.07; (d): sample mean from (a); (f): sample mean from (b).



Figure 8: Image Editing Samples with Stable Diffusion 1.5, the source prompt is given by 'a high-quality portrait of a man', and the target prompt is given by 'a high-quality portrait of a woman', the target MSE level is given by 0.10



Figure 9: Image Editing Samples with Stable Diffusion 1.5, the source prompt is given by 'a high-quality portrait of an old man', and the target prompt is given by 'a high-quality portrait of a young man', the target MSE level is given by 0.09

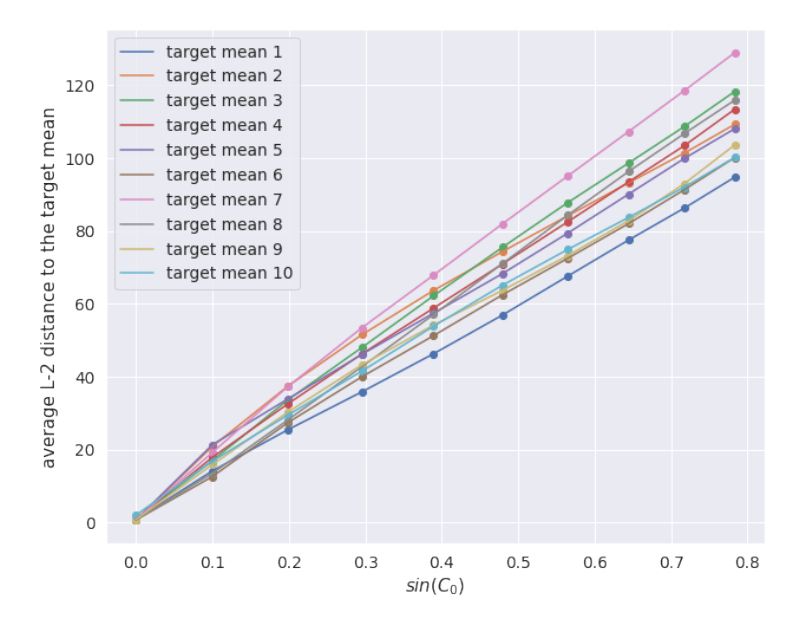


Figure 10: We first sample 50 images around each target mean in the FFHQ dataset. We then obtain the DDIM inverse of each target mean, and then add spherical perturbation to it. When the scale of perturbations  $\sin(C_0)$  increases, the average of norms of the residuals between each sample and the target mean approximately increases linearly.



Figure 11: We demonstrate that there is sudden change in output when testing on OOD input perturbed with increasing Gaussian noise. The backbone model is a pixel diffusion model (DDPM++), which is only trained on FFHQ. The top row uses an OOD input from ImageNet, and the bottom row uses an image from FFHQ validation set input.  $C_0$  from left to right: 0.0, 0.2, 0.4, 0.6, 0.8

# **NeurIPS Paper Checklist**

#### 1. Claims

Question: Do the main claims made in the abstract and introduction accurately reflect the paper's contributions and scope?

Answer: [Yes]

Justification: The contribution and scope are stated in the introduction.

Guidelines:

- The answer NA means that the abstract and introduction do not include the claims made in the paper.
- The abstract and/or introduction should clearly state the claims made, including the
  contributions made in the paper and important assumptions and limitations. A No or
  NA answer to this question will not be perceived well by the reviewers.
- The claims made should match theoretical and experimental results, and reflect how much the results can be expected to generalize to other settings.
- It is fine to include aspirational goals as motivation as long as it is clear that these goals are not attained by the paper.

#### 2. Limitations

Question: Does the paper discuss the limitations of the work performed by the authors?

Answer: [Yes].

Justification: We have provided a discussion about limitations in the conclusion section.

#### Guidelines:

- The answer NA means that the paper has no limitation while the answer No means that the paper has limitations, but those are not discussed in the paper.
- The authors are encouraged to create a separate "Limitations" section in their paper.
- The paper should point out any strong assumptions and how robust the results are to violations of these assumptions (e.g., independence assumptions, noiseless settings, model well-specification, asymptotic approximations only holding locally). The authors should reflect on how these assumptions might be violated in practice and what the implications would be.
- The authors should reflect on the scope of the claims made, e.g., if the approach was only tested on a few datasets or with a few runs. In general, empirical results often depend on implicit assumptions, which should be articulated.
- The authors should reflect on the factors that influence the performance of the approach. For example, a facial recognition algorithm may perform poorly when image resolution is low or images are taken in low lighting. Or a speech-to-text system might not be used reliably to provide closed captions for online lectures because it fails to handle technical jargon.
- The authors should discuss the computational efficiency of the proposed algorithms and how they scale with dataset size.
- If applicable, the authors should discuss possible limitations of their approach to address problems of privacy and fairness.
- While the authors might fear that complete honesty about limitations might be used by reviewers as grounds for rejection, a worse outcome might be that reviewers discover limitations that aren't acknowledged in the paper. The authors should use their best judgment and recognize that individual actions in favor of transparency play an important role in developing norms that preserve the integrity of the community. Reviewers will be specifically instructed to not penalize honesty concerning limitations.

#### 3. Theory assumptions and proofs

Question: For each theoretical result, does the paper provide the full set of assumptions and a complete (and correct) proof?

Answer: [Yes]

Justification: We have clearly stated our assumptions, propositions and results in Sec. 3 and 4, with proof in the Appendix.

#### Guidelines:

- The answer NA means that the paper does not include theoretical results.
- All the theorems, formulas, and proofs in the paper should be numbered and crossreferenced
- All assumptions should be clearly stated or referenced in the statement of any theorems.
- The proofs can either appear in the main paper or the supplemental material, but if they appear in the supplemental material, the authors are encouraged to provide a short proof sketch to provide intuition.
- Inversely, any informal proof provided in the core of the paper should be complemented by formal proofs provided in appendix or supplemental material.
- Theorems and Lemmas that the proof relies upon should be properly referenced.

#### 4. Experimental result reproducibility

Question: Does the paper fully disclose all the information needed to reproduce the main experimental results of the paper to the extent that it affects the main claims and/or conclusions of the paper (regardless of whether the code and data are provided or not)?

Answer: [Yes]

Justification: We have fully explained the setup of our experiments in Sec. 5.

#### Guidelines:

- The answer NA means that the paper does not include experiments.
- If the paper includes experiments, a No answer to this question will not be perceived well by the reviewers: Making the paper reproducible is important, regardless of whether the code and data are provided or not.
- If the contribution is a dataset and/or model, the authors should describe the steps taken to make their results reproducible or verifiable.
- Depending on the contribution, reproducibility can be accomplished in various ways. For example, if the contribution is a novel architecture, describing the architecture fully might suffice, or if the contribution is a specific model and empirical evaluation, it may be necessary to either make it possible for others to replicate the model with the same dataset, or provide access to the model. In general, releasing code and data is often one good way to accomplish this, but reproducibility can also be provided via detailed instructions for how to replicate the results, access to a hosted model (e.g., in the case of a large language model), releasing of a model checkpoint, or other means that are appropriate to the research performed.
- While NeurIPS does not require releasing code, the conference does require all submissions to provide some reasonable avenue for reproducibility, which may depend on the nature of the contribution. For example
- (a) If the contribution is primarily a new algorithm, the paper should make it clear how to reproduce that algorithm.
- (b) If the contribution is primarily a new model architecture, the paper should describe the architecture clearly and fully.
- (c) If the contribution is a new model (e.g., a large language model), then there should either be a way to access this model for reproducing the results or a way to reproduce the model (e.g., with an open-source dataset or instructions for how to construct the dataset).
- (d) We recognize that reproducibility may be tricky in some cases, in which case authors are welcome to describe the particular way they provide for reproducibility. In the case of closed-source models, it may be that access to the model is limited in some way (e.g., to registered users), but it should be possible for other researchers to have some path to reproducing or verifying the results.

#### 5. Open access to data and code

Question: Does the paper provide open access to the data and code, with sufficient instructions to faithfully reproduce the main experimental results, as described in supplemental material?

Answer: [Yes]

Justification: This paper utilizes publicly available datasets, with detailed access instructions and appropriate citations provided. While the code is not publicly released at the time of submission, we intend to make it available upon acceptance of the paper.

#### Guidelines:

- The answer NA means that paper does not include experiments requiring code.
- Please see the NeurIPS code and data submission guidelines (https://nips.cc/public/guides/CodeSubmissionPolicy) for more details.
- While we encourage the release of code and data, we understand that this might not be
  possible, so "No" is an acceptable answer. Papers cannot be rejected simply for not
  including code, unless this is central to the contribution (e.g., for a new open-source
  benchmark).
- The instructions should contain the exact command and environment needed to run to reproduce the results. See the NeurIPS code and data submission guidelines (https://nips.cc/public/guides/CodeSubmissionPolicy) for more details.
- The authors should provide instructions on data access and preparation, including how to access the raw data, preprocessed data, intermediate data, and generated data, etc.
- The authors should provide scripts to reproduce all experimental results for the new proposed method and baselines. If only a subset of experiments are reproducible, they should state which ones are omitted from the script and why.
- At submission time, to preserve anonymity, the authors should release anonymized versions (if applicable).
- Providing as much information as possible in supplemental material (appended to the paper) is recommended, but including URLs to data and code is permitted.

### 6. Experimental setting/details

Question: Does the paper specify all the training and test details (e.g., data splits, hyperparameters, how they were chosen, type of optimizer, etc.) necessary to understand the results?

Answer: [Yes]

Justification: It is clearly stated in the experiment section (Sec. 5).

# Guidelines:

- The answer NA means that the paper does not include experiments.
- The experimental setting should be presented in the core of the paper to a level of detail that is necessary to appreciate the results and make sense of them.
- The full details can be provided either with the code, in appendix, or as supplemental material.

# 7. Experiment statistical significance

Question: Does the paper report error bars suitably and correctly defined or other appropriate information about the statistical significance of the experiments?

Answer: [Yes]

Justification: We have reported multiple metrics in our experiments with average values in main paper and the standard deviations in Appendix.

- The answer NA means that the paper does not include experiments.
- The authors should answer "Yes" if the results are accompanied by error bars, confidence intervals, or statistical significance tests, at least for the experiments that support the main claims of the paper.
- The factors of variability that the error bars are capturing should be clearly stated (for example, train/test split, initialization, random drawing of some parameter, or overall run with given experimental conditions).
- The method for calculating the error bars should be explained (closed form formula, call to a library function, bootstrap, etc.)

- The assumptions made should be given (e.g., Normally distributed errors).
- It should be clear whether the error bar is the standard deviation or the standard error
  of the mean.
- It is OK to report 1-sigma error bars, but one should state it. The authors should preferably report a 2-sigma error bar than state that they have a 96% CI, if the hypothesis of Normality of errors is not verified.
- For asymmetric distributions, the authors should be careful not to show in tables or figures symmetric error bars that would yield results that are out of range (e.g. negative error rates).
- If error bars are reported in tables or plots, The authors should explain in the text how they were calculated and reference the corresponding figures or tables in the text.

# 8. Experiments compute resources

Question: For each experiment, does the paper provide sufficient information on the computer resources (type of compute workers, memory, time of execution) needed to reproduce the experiments?

Answer: [Yes]

Justification: We provide the information about computer resoures in Appendix.

#### Guidelines:

- The answer NA means that the paper does not include experiments.
- The paper should indicate the type of compute workers CPU or GPU, internal cluster, or cloud provider, including relevant memory and storage.
- The paper should provide the amount of compute required for each of the individual experimental runs as well as estimate the total compute.
- The paper should disclose whether the full research project required more compute than the experiments reported in the paper (e.g., preliminary or failed experiments that didn't make it into the paper).

#### 9. Code of ethics

Question: Does the research conducted in the paper conform, in every respect, with the NeurIPS Code of Ethics https://neurips.cc/public/EthicsGuidelines?

Answer: [Yes]

Justification: The research complies fully with the NeurIPS Code of Ethics. It does not involve sensitive data, human subjects, or potentially harmful applications.

Guidelines: The research complies fully with the NeurIPS Code of Ethics. It does not involve sensitive data, human subjects, or potentially harmful applications.

# Guidelines:

- The answer NA means that the authors have not reviewed the NeurIPS Code of Ethics.
- If the authors answer No, they should explain the special circumstances that require a deviation from the Code of Ethics.
- The authors should make sure to preserve anonymity (e.g., if there is a special consideration due to laws or regulations in their jurisdiction).

#### 10. Broader impacts

Question: Does the paper discuss both potential positive societal impacts and negative societal impacts of the work performed?

Answer: [NA].

Justification: This paper presents work whose goal is to advance the field of generative AI. There are many potential societal consequences of our work, none which we feel must be specifically highlighted here.

- The answer NA means that there is no societal impact of the work performed.
- If the authors answer NA or No, they should explain why their work has no societal impact or why the paper does not address societal impact.

- Examples of negative societal impacts include potential malicious or unintended uses (e.g., disinformation, generating fake profiles, surveillance), fairness considerations (e.g., deployment of technologies that could make decisions that unfairly impact specific groups), privacy considerations, and security considerations.
- The conference expects that many papers will be foundational research and not tied to particular applications, let alone deployments. However, if there is a direct path to any negative applications, the authors should point it out. For example, it is legitimate to point out that an improvement in the quality of generative models could be used to generate deepfakes for disinformation. On the other hand, it is not needed to point out that a generic algorithm for optimizing neural networks could enable people to train models that generate Deepfakes faster.
- The authors should consider possible harms that could arise when the technology is being used as intended and functioning correctly, harms that could arise when the technology is being used as intended but gives incorrect results, and harms following from (intentional or unintentional) misuse of the technology.
- If there are negative societal impacts, the authors could also discuss possible mitigation strategies (e.g., gated release of models, providing defenses in addition to attacks, mechanisms for monitoring misuse, mechanisms to monitor how a system learns from feedback over time, improving the efficiency and accessibility of ML).

# 11. Safeguards

Question: Does the paper describe safeguards that have been put in place for responsible release of data or models that have a high risk for misuse (e.g., pretrained language models, image generators, or scraped datasets)?

Answer: [NA]

Justification: The paper does not introduce or release any new models or datasets that could pose a risk of misuse.

#### Guidelines:

- The answer NA means that the paper poses no such risks.
- Released models that have a high risk for misuse or dual-use should be released with
  necessary safeguards to allow for controlled use of the model, for example by requiring
  that users adhere to usage guidelines or restrictions to access the model or implementing
  safety filters.
- Datasets that have been scraped from the Internet could pose safety risks. The authors should describe how they avoided releasing unsafe images.
- We recognize that providing effective safeguards is challenging, and many papers do
  not require this, but we encourage authors to take this into account and make a best
  faith effort.

#### 12. Licenses for existing assets

Question: Are the creators or original owners of assets (e.g., code, data, models), used in the paper, properly credited and are the license and terms of use explicitly mentioned and properly respected?

Answer: [Yes].

Justification: We have properly cited and credited the pretrained diffusion models (Stable Diffusion 1.5), and datasets used in our work.

- The answer NA means that the paper does not use existing assets.
- The authors should cite the original paper that produced the code package or dataset.
- The authors should state which version of the asset is used and, if possible, include a URL.
- The name of the license (e.g., CC-BY 4.0) should be included for each asset.
- For scraped data from a particular source (e.g., website), the copyright and terms of service of that source should be provided.

- If assets are released, the license, copyright information, and terms of use in the
  package should be provided. For popular datasets, paperswithcode.com/datasets
  has curated licenses for some datasets. Their licensing guide can help determine the
  license of a dataset.
- For existing datasets that are re-packaged, both the original license and the license of the derived asset (if it has changed) should be provided.
- If this information is not available online, the authors are encouraged to reach out to the asset's creators.

#### 13. New assets

Question: Are new assets introduced in the paper well documented and is the documentation provided alongside the assets?

Answer: [NA].

Justification: At the time of submission, we have not released any new assets, but after acceptance, we will release new assets including code and trained models along with detailed documentation for them.

#### Guidelines:

- The answer NA means that the paper does not release new assets.
- Researchers should communicate the details of the dataset/code/model as part of their submissions via structured templates. This includes details about training, license, limitations, etc.
- The paper should discuss whether and how consent was obtained from people whose asset is used.
- At submission time, remember to anonymize your assets (if applicable). You can either create an anonymized URL or include an anonymized zip file.

# 14. Crowdsourcing and research with human subjects

Question: For crowdsourcing experiments and research with human subjects, does the paper include the full text of instructions given to participants and screenshots, if applicable, as well as details about compensation (if any)?

Answer: [NA].

Justification: The paper does not involve crowdsourcing nor research with human subjects.

#### Guidelines:

- The answer NA means that the paper does not involve crowdsourcing nor research with human subjects.
- Including this information in the supplemental material is fine, but if the main contribution of the paper involves human subjects, then as much detail as possible should be included in the main paper.
- According to the NeurIPS Code of Ethics, workers involved in data collection, curation, or other labor should be paid at least the minimum wage in the country of the data collector.

# 15. Institutional review board (IRB) approvals or equivalent for research with human subjects

Question: Does the paper describe potential risks incurred by study participants, whether such risks were disclosed to the subjects, and whether Institutional Review Board (IRB) approvals (or an equivalent approval/review based on the requirements of your country or institution) were obtained?

Answer: [NA].

Justification: The paper does not involve crowdsourcing nor research with human subjects.

#### Guidelines:

 The answer NA means that the paper does not involve crowdsourcing nor research with human subjects.

- Depending on the country in which research is conducted, IRB approval (or equivalent)
  may be required for any human subjects research. If you obtained IRB approval, you
  should clearly state this in the paper.
- We recognize that the procedures for this may vary significantly between institutions and locations, and we expect authors to adhere to the NeurIPS Code of Ethics and the guidelines for their institution.
- For initial submissions, do not include any information that would break anonymity (if applicable), such as the institution conducting the review.

#### 16. Declaration of LLM usage

Question: Does the paper describe the usage of LLMs if it is an important, original, or non-standard component of the core methods in this research? Note that if the LLM is used only for writing, editing, or formatting purposes and does not impact the core methodology, scientific rigorousness, or originality of the research, declaration is not required.

Answer: [NA].

Justification: The core methods and contributions of the paper do not involve the use of LLM in any important, original, or non-standard way.

- The answer NA means that the core method development in this research does not involve LLMs as any important, original, or non-standard components.
- Please refer to our LLM policy (https://neurips.cc/Conferences/2025/LLM) for what should or should not be described.